PHYSICS

FINAL REPORT
SRB SEAWATER CORROSION PROJECT
July, 1991
(NAS8-38800)

Auburn University, Solid State Sciences Center,
Department of Physics

M. J. Bozack

AUBURN UNIVERSITY

AUBURN, ALABAMA

FINAL REPORT
SRB SEAWATER CORROSION PROJECT
July, 1991
(NAS8-38800)

Auburn University, Solid State Sciences Center,
Department of Physics

M. J. Bozack

Abstract

The corrosion behavior of 2219 aluminum when exposed to seawater has been characterized. Controlled corrosion experiments at three different temperatures (T = 30 C, 60 C and 100 C) and two different environments (seawater and 3.5 % salt solution) have been designed to elucidate the initial stages in the corrosion process. We find that 2219 aluminum is an active catalytic surface for growth of Al_2O_3, NaCl, and MgO. Formation of Al_2O_3 if favored at lower temperatures, while MgO is favored at higher temperatures. Visible corrosion products are formed within 30 minutes after seawater exposure. Corrosion characteristics in 3.5% salt solution are different than corrosion in seawater, casting doubt on the common practice of simulating corrosive effects in seawater by substituting 3.5% salt solutions. Techniques utilized have been: i) scanning electron microscopy (SEM); ii) energy dispersive X-ray spectroscopy (EDX); and iii) Auger electron spectroscopy (AES). The results suggest that corrosion may be minimized by utilizing a less reactive aluminum alloy, by rinsing the aluminum as soon as possible after retrieval, and/or by using a protective coating on the 2219 alloy.

TABLE OF CONTENTS

FINAL REPORT -- SRB SEAWATER CORROSION PROJECT
July, 1991
(NAS8-38800)

Auburn University, Solid State Sciences Center, Department of Physics

M. J. Bozack

I. Introduction

The goal of this research effort has been to characterize the corrosion behavior of 2219 aluminum when exposed to seawater. Specifically, we have performed controlled corrosion experiments at three different temperatures (T = 30 C, 60 C and 100 C) and two different environments (seawater and 3.5 % salt solution) to elucidate the initial stages in the corrosion process. The experimental matrix is detailed below. Techniques utilized have been: i) scanning electron microscopy (SEM); ii) energy dispersive X-ray spectroscopy (EDX); and iii) Auger electron spectroscopy (AES). We find that 2219 aluminum is an active catalytic surface for growth of Al_2O_3, NaCl, and MgO. Formation of Al_2O_3 if favored at lower temperatures, while MgO is favored at higher temperatures. Visible corrosion products are formed within 30 minutes after seawater exposure. Corrosion characteristics in 3.5% salt solution are different than corrosion in seawater, casting doubt on the common practice of simulating corrosive effects in seawater by substituting 3.5% salt solutions. The results suggest that corrosion may be minimized by utilizing a less reactive aluminum alloy, by rinsing the AFT skirt as soon as possible after retrieval, and/or by using a protective coating on the 2219 alloy.

Part II of this report discusses the general corrosive behavior of aluminum in seawater, the formation of protective oxide on aluminum, and the influence of environmental factors on aluminum corrosion. Part III deals with experimental methods, apparatus details, and specimen preparation. Part IV details the Al-Cu alloy microstructure and composition before corrosive exposure. Parts V-VII discusses the results of specific corrosion experiments in seawater and 3.5% salt solution. A final section offers suggestion for reducing corrosion.

II. The Corrosion Process

Corrosion may be defined as the chemical reaction of a metal with a nonmetal in the surrounding environment, with the formation of compounds which are referred to as corrosion products. Since metals are used for engineering applications because of their unique mechanical properties (e.g., strength, hardness, and ductility), conversion of the metal into a powdery, non-adherent compound, if allowed to proceed, will result in the deterioration of the metallic component. The degree to which this occurs depends on the rate of the corrosion reaction, which determines the extent of conversion of the metal into corrosion products over a given period of time.

In addition to factors such as metal purity, environment, and the intrinsic nature of the material, the corrosion product is an important factor in controlling the rate of corrosion. For example, while metallic zinc is less stable than metallic iron, it is more resistant to corrosion in a number of enviroinments. This is explained by the fact that the corrosion products of Zn are more protective than those of Fe, and this phenomenon applies even greater to metals such as Al, Ti, and Ta, which, although thermodynamically highly unstable, form very protective films of metal oxide.

The role of the corrosion product in acting as a protective barrier can be illustrated by comparing the high-temperature oxidation of iron with its corrosion in an oxygen-containing aqueous solution such as water. It is well-known that heating iron in air results in the formation of temper coloration (blue). This is due to the formation of a transparent film of oxide.

To give a common example, the rusting of Fe is known to involve oxygen. Iron does not rust in water unless O_2 is present. Rusting also involves H_2O; iron does not rust in oil, even if it contains O_2, unless H_2O is also present. Other factors such as the pH of the solution, the presence of salts, contact with metals more difficult to oxidize than iron, and stress on the iron can accelerate rusting.

The corrosion of iron is generally believed to be electrochemical in nature. A region on the surface of the iron serves as an anode at which undergoes oxidation:

$$Fe(s) \rightarrow Fe^{+2}(aq) + 2e^{-} \; ; \; E_{ox} = 0.44 \text{ eV}$$

The electrons so produced migrate through the metal to another portion of the surface that serves as the cathode. Here oxygen can be reduced:

$$O_2(g) + 4H^+(aq) + 4e^- \rightarrow 2\,H_2O \;\; ; \;\; E_{red} = 1.23\ eV$$

Notice that H^+ is involved in the reduction of O_2. As the concentration of H^+ is lowered (that is, as the pH is increased), the reduction of O_2 becomes less favorable. It is observed that iron in contact with a solution whose pH is above 9-10 does not corrode. In the course of the corrosion, the Fe^{+2} formed at the anode is further oxidized to Fe^{+3}. The Fe^{+3} forms the hydrated iron(III) oxide known as rust:

$$4Fe^{+2}(aq) + O_2(g) + 4\,H_2O + 2xH_2O \rightarrow 2Fe_2O_3 \cdot xH_2O(s) + 8H^+(aq)$$

Because the cathode is generally the area having the largest supply of O_2, the rust often deposits there. If you look closely at a shovel after it has stood outside in the moist air with wet dirt adhered to its blade, you may notice that pitting has occurred under the dirt but that rust has formed elsewhere, where O_2 is more readily available.

The enhanced corrosion caused by the presence of salts is usually evident on autos in areas where there is heavy salting of roads during winter. The effect of salts is readily explained by the voltaic mechansm: the ions of a salt provide the electrolyte necessary for completion of the electrical circuit.

The presence of anodic and cathodic sites on the iron requires two different chemical environments on the surface. These can occur through the presence of impurities or lattice defects (perhaps introduced by strain on the metal). At the sites of such impurities or defects the atomic level environment around the iron atom may permit the metal to be either more or less easily oxidized that at normal lattice sites. Thus these sites may serve as either anodes or cathodes. Ultrapure iron, prepared in such a way as to minimize lattice defects, is far less susceptible to corrosion than is ordinary iron.

Iron is often covered with a coat of point or another metal such as Sn, Zn, or Cr to protect its surface against corrosion. For example, tin cans are produced by applying a thin layer of Sn over steel. The Sn protects the iron only as long as the protective layer remains intact. Once it is broken and the iron exposed to air and water, tin actually promotes the corrosion of the iron. It does so by serving as the cathode in the electrochemical corrosion. As shown by the following half-cell potentials, iron is more readily oxidized than tin:

$$Fe(s) \rightarrow Fe^{+2}(aq) + 2e^{-} ; E_{ox} = 0.44 \text{ eV}$$

$$Sn(s) \rightarrow Sn^{+2}(aq) + 2e^{-} ; E_{ox} = 0.14 \text{ eV}$$

The iron therefore serves as the anode and is oxidized.

Galvanized iron is produced by coating iron with a thin layer of zinc. The Zn protects the iron against corrosion even after the surface coat is broken. In this case the Fe serves as the cathode in the electrochemical corrosion because Zn is oxidized more easily the Fe:

$$Zn(s) \rightarrow Zn^{+2}(aq) + 2e^{-} ; E_{ox} = 0.76 \text{ eV}$$

The Zn therefore serves as the anode and is corroded instead of the Fe. Such protection of a metal by making it the cathode in an electrochemical cell is known as cathodic protection. Underground pipelines are often protected against corrosion by making the pipeline the cathode of a voltaic cell. Pieces of an active metal such as Mg are buried along the pipeline and connected to it by wire. In moist soil, where corrosion can occur, the active metal serves as the anode and the pipe experiences cathodic protection.

The discussion above has centered on iron, but similar consideration hold for most corrosion processes. To one final example, an aluminum can disposed of carelessly beside the road will last much longer than a steel can. On the basis of the standard oxidation potentials of Al (E_{ox} = 1.66 V) and Fe (E_{ox} = 0.44 V), one would expect the Al to be much more readily corroded. The slow corrosion of Al is explained by the formation of a thin oxide coating that forms on its surface. This protects the underlying metal from further corrosion. Magnesium, which also has a large oxidation potential, is similarly protected. The oxide coat on iron is too porous to offer similar protection. However, when iron is alloyed with chromium, a protective oxide coating does form. This is stainless steel.

A. <u>The Surface Oxide on Aluminum</u>

The properties of the aluminum oxide film provide aluminum and its alloys with its resistance to corrosion. When a fresh aluminum surface is created and exposed to air, it oxidizes rapidly and acquires an adherent, protective film of aluminum oxide (i.e., alumina) which tends to resist further oxidation. Aluminum

oxide is relatively inert chemically, and it is on this inactivity that the good corrosion resistance of aluminum depends. When the oxide film dissolves, as it does in the presence of certain chemicals, dissolution of the metal also occurs and the metal corrodes uniformly. Alternatively, when the film is damaged under conditions that prevent normal self healing, localized corrosion ensues. This corrosion may take the form of pitting or intergranular attack.

It is commonly believed that the oxide film is stable over a pH range of about 4.5 to 8.5, but several exceptions to this rule of thumb can be identified. For example, aluminum is rapidly attacked in NaOH solutions not far from neutrality (pH 7), whereas it is resistant to NH_3OH even at pH 13. Other exceptions include the resistance of aluminum to concentrated nitric acid at pH 1 and to glacial acetic acid at pH 5. The film, however, is dissolved in most strong acids and alkalis. Hence, although aluminum alloys may be attacked outside the pH range 4.5 - 8.5, this is usually not a problem under normal marine situations.

Normal air-exposed aluminum is covered by an amorphous aluminum oxide (Al_2O_3) film which is believed to exist in various degrees of hydration ($Al_2O_3 \cdot xH_2O$) depending on its relative humidity and temperature of formation. When the aluminum is exposed to a moist atmosphere or is immersed in water, the oxide film thickens, meaning the growth rate is much more rapid in water. In both cases the rate of growth increases with temperature. The composition and structure of the hydrated oxide films formed in water has been discussed by Tragert [1]. There are six common crystalline forms of aluminum oxide: gibbsite (α-$Al_2O_3 \cdot 3H_2O$), bayerite (β-$Al_2O_3 \cdot 3H_2O$), boehmite (α-$Al_2O_3 \cdot H_2O$), diaspore (β-$Al_2O_3 \cdot H_2O$), gamma alumina (γ-Al_2O_3), corundum (α-Al_2O_3). Of these, bayerite is the usual corrosion product film that forms on aluminum in water at moderate temperatures ($T < 85$ C).

The physical aspects of the oxide film on aluminum have been discussed by Troutner [2] and by Hunter and Fowle [3]. When aluminum is exposed to air, a duplex film is formed. This duplex film consists of a thin, protective, nonporous, "barrier" film, immediately adjacent to the metal surface, and a more permeable outer bulk film. The barrier film rapidly reaches a maximum thickness, which in the case of oxidation in air is dependent on the temperature. The limiting barrier thickness is the same for oxygen, dry air, and moist air. The barrier portion may comprise most of the film formed in dry air, while in water the bulk film grows much thicker. For example, after a short time in water at 300 C, the bulk film

may be 750 Å thick, while the thickness of the barrier portion is only 35 Å. Although the barrier film controls the rate of oxidation in dry air, there is strong evidence that the rate of film growth in water is controlled by the thickness of the bulk film. Differences in corrosion rates in different aqueous environments appear to be caused by differences in the solubility of the bulk film.

When aluminum is immersed in water, the oxide film thickens rapidly, at a rate that increases with temperature, but even at 20 C it is many times more rapid in water than in air. For example, Hart [4] reported a thickness of 55,000 Å for 1099 aluminum (99.99%) immersed in distilled water for 20 days. On the other hand, Barker and Godard [5] found a thickness of 4800 Å for 1099 aluminum immersed in alumina-saturated tap water for 22 days, suggesting that water purity has a marked influence on the rate of film formation. The rate of oxide growth decreases with time, and reaches a limiting thickness which depends on the temperature, the oxygen content of the water, the ions present, and the pH. The degree of hydration of the oxide film is dependent on the water temperature. It has been suggested that the initial corrosion product is aluminum hydroxide, $Al(OH)_3$, which ages with time to become a hydrated oxide or mixture of oxides, $Al_2O_3 \cdot H_2O$, but this is unconfirmed. What can be said is that the growth of the oxide film on aluminum in water is complex and greatly influenced by the temperature, the ions present, and the duration of exposure. The bulk of experimental data suggest that the thickened oxide films developed in pure water at room temperature increase the resistance of the surface to corrosion. If such films can be developed before some corrosive conditions are encountered, no corrosion will occur, whereas a freshly exposed surface with only an air-formed film with be subject to corrosion.

B. Properties of Seawater

The most characteristic feature of seawater is its high salt content. The salt content of seawater is remarkably constant; the common average value used for open ocean water is about 35 parts per thousand. In addition, the saline composition, regardless of the absolute concentration, has virtually constant proportions for the different major constituents (see Table I). However, some of the other constituents of importance to the corrosion reaction such as the percentage of dissolved oxygen and CO_2 do vary and, of course, properties such as temperature, density, and electrical conductivity are not constant. The temperature of seawater varies directly with latitude, and the range is from

about -2 C at the poles to 35 C at the equator. The amount of dissolved gases varies with temperature from about 8 ml/l for surface waters in the Arctic to about 4.5 ml/l in the tropics. In seawater, the CO_2 is present as bicarbonate and carbonate ions, as undissociated molecules of CO_2, and as H_2CO_3 molecules which are in equilibrium with each other in solution. The free CO_2 exerts a partial pressure which is related to temperature and pH. When the pH of the seawater rises at a constant temperature, CO_2 is released and enters the atmosphere, the free CO_2 in solution falls, and the amount of carbonate increases. One of the results of this complicated series of reactions is that seawater is able to resist changes in its pH, i.e., it is a highly buffered solution.

Seawater is normally alkaline and the pH of the surface layers of the ocean, where the water is in equilibrium with the CO_2 of the atmosphere, lies between 8.1 and 8.3. The presence of large quantities of hydrogen sulfide tends to lower the pH value (the water becomes more acidic), while if there is considerable photosynthetic activity of plants, which reduces the CO_2 content of the water, higher pH values will be found (the water becomes more alkaline). The pH of seawater is altered by variations in temperature. The usual effect of a rise in temperature is to reduce the pH. In the ocean depths, the pH is usually below 8.0 because of the effect of pressure.

Table I

Average Concentrations of the Principal Ions in Seawater[a]
(parts per thousand by weight)

Ion	% by Weight	
chloride, Cl^-	18.980	
sulphate, SO_4^{-2}	2.649	
bicarbonate, HCO_3^-	0.140	
bromide, Br^-	0.065	
borate, $H_2BO_3^-$	0.026	
fluoride, F^-	0.001	
Anions Total		21.861 %
sodium, Na^+	10.556	
magnesium, Mg^{+2}	1.272	
calcium, Ca^{+2}	0.400	
potassium, K^+	0.380	
strontium, Sr^{+2}	0.013	
Cations Total		12.621 %
Overall total salinity		34.482 %

[a] Source: Seawater: Its Composition, Properties, and Behavior, J. Brown, Pergamon, 1989, p. 30.

C. General Corrosion Behavior of Aluminum in Seawater

The main practical interest in aluminum corrosion resides not in the corrosion behavior of pure aluminum but in the performance of specific aluminum alloys. Because the addition of alloying elements to aluminum affects its corrosion resistance, it is difficult to make general statements concerning the corrosion behavior of aluminum. Nevertheless, it is instructive to consider some generalizations regarding the corrosion of aluminum.

1. Aluminum Alloys in General

A number of general papers have been written on the corrosion resistance of aluminum alloys [6-17]. In general, aluminum alloys have good corrosion resistance in the following environments: atmosphere, fresh water, seawater, soils, and many chemicals. The corrosion resistance derives from the adherent protective oxide film formed on the surface when aluminum is exposed to oxidizing solutions. We will focus on its behavior in seawater. Aluminum has been used in marine craft for decades. The first use was by the Wellman Arctic expeditions of 1896 [18] in the form of sledges and aluminum boats. About 1900, aluminum was used in the superstructure of U.S. Navy torpedo boats [19]. Some of the early examples suffered extensive corrosion due to unfavorable alloy composition or galvanic corrosion, which were not well understood at the time, and this deterred others from using aluminum alloys for marine construction for some time. The use of aluminum was continued in the thirties by several ship manufacturers. One early all-aluminum boat still in service is the Interceptor, a patrol boat built in Canada in 1933. Since 1945, aluminum canoes, rowboats, and pleasure craft have been produced by the tens of thousands annually. For inland or marine service these are either left bare or painted, depending on the appearance desired. Hundreds of Al-seagoing patrol boats, torpedo boats, ferries, yachts, and hydrofoils have also been built with aluminum hulls.

The most extensive published results of seawater corrosion tests on aluminum alloys appears to be the work of Godard and Booth [20]. The conclusion of this study was that the Al-Mg alloys (AA-5052, AA-5083, AA-5086, AA-5154, and AA-5056) and Al-Mn alloys (AA-3003, AA-3004) are

the most resistant to seawater. There is negligible thinning due to uniform corrosion, and the bulk weight loss corrosion rate amounts to less than 0.2 mils per year, or 1/20 that for steel in seawater. The Al-Mg-Si alloys (AA-6051, AA-6061, AA-6063) are somewhat less resistant to seawater. The density of pitting is higher, the pits tend to be larger, and there may be a tendency toward intergranular corrosion. Some blistering of the surface appears to occur. However, there is no general thinning and the weight loss corrosion rate is on the order of 0.5 mils per year.

During the war years, a divergence of opinion developed between Britain and America as to the most suitable aluminum alloy for marine construction. In the U.S., Alcoa developed the Al-Mg-Si alloy AA-6061, which contained 0.25% Cu. In England, on the other hand, there was a reluctance to use a Cu-containing alloy, since Cu was known to reduce corrosion resistance. Instead, Al-Mg-Si alloys (with Si in excess of that required to form Mg_2Si), for example AA-6053 were used, and binary Al-Mg alloys were introduced. In America, the Al-Mg-Si alloy was rejected as being unduly subject to intergranular corrosion. The argument has become largely academic, since Al-Mg alloys are now preferred for use in seawater in all parts of the world.

The stronger aircraft alloys (Al-Cu and Al-Zn-Mg-Cu) are considered to have poor corrosion resistance to seawater, and in the unprotected state a 0.250 inch plate will perforate in a few years. However, if protected by cladding, metal spraying, or paint, these alloys exhibit excellent resistance to seawater.

In summary, the available information clearly indicates that selected aluminum alloys, especially the binary alloys containing magnesium, have a high degree of resistance to corrosion by seawater, and that in the absence of dissimilar metals, marine structures built from them will have a long life, even if no corrosion-prevention measures are taken.

2. The Al-Cu Alloy System

Typical wrought alloys in the Al-Cu system are AA-2011, 2014, 2024, and 2219, which have the following compositions:

AA Number	% Cu	% Si	% Mn	% Mg
2011	5.5	0.4	---	---
2014	4.4	0.8	0.8	0.5
2017	4.0	0.8	0.7	0.5
2024	4.4	0.5	0.6	1.5
2219	6.3	0.2	0.3	0.02

When metallurgists began to try to improve the strength of aluminum, copper was one of the first alloying elements they employed, and Al-Cu alloys were used before the turn of the century. These alloys had, in general, poor resistance to corrosion, and it was not until about 1911 that researchers found that the addition of about 0.5% Mg improved the corrosion resistance and at the same time produced an age-hardened alloy group which came to be known as "duralumin," of which AA 2017 is typical.

Copper usually begins to show its influence in very small amounts; even 0.005% Cu has a detectable effect. The detrimental influence of 0.15% Cu can easily be measured in laboratory corrosion tests. In general, Al-Cu alloys have relatively poor corrosion resistance, and require surface protection when used in corrosive environments. Without protection, they suffer extensive corrosion in marine and industrial environments. When Al-Cu alloys must be used, they are frequently cladded with pure aluminum and heat treated to obtain the maximum resistance to corrosion.

In the heat-treated condition of Al-Cu alloys, the copper is almost entirely in solid solution after quenching. When the alloy is aged at room temperature, the Cu atoms gather as Guinier-Preston zones, and eventually form intermediate pre-precipitation phases. Precipitation heat treatment

produces further formation of these phases and some of the alloy transforms into stable $CuAl_2$. Faulty heat treatment or subsequent reheating with uncontrolled cooling may precipitate additional $CuAl_2$, which may concentrate in the grain boundaries and give rise to a high degree of susceptibility to intergranular corrosion and stress corrosion.

C. The Influence of Environmental Factors on Aluminum Corrosion

1. Water

Except in cases of high-temperature oxidation and gas-metal reactions, there is no corrosion of aluminum unless water is present. In general, the water must contain oxygen or air; if oxygen is removed, corrosion ceases. Water is beneficial in some cases. Aluminum exposed to an aggressive marine or industrial atmosphere will last longer if it is rained on frequently, since the water dilutes and washes away corrosive residues of salt or soot.

2. Temperature

An increase in temperature has a strong accelerating effect on the corrosion of aluminum unless the heat increases the rate of drying and thus the period of wetness. For example, aluminum overhead transmission cables which operate above atmospheric temperature usually last indefinitely due to the drying effect.

3. Agitation

Agitation of a corrosive liquid or gas in contact with aluminum usually accelerates the rate of corrosion. Velocities greater than about 8 feet per minute are, however, beneficial and may prevent pitting [21].

4. Surface-to-Volume Ratio

The surface-to-volume ratio of a metal has a marked influence on corrosion. If the ratio is high, the metal deteriorates more rapidly than it does when the ratio is low. For example, the rate of loss of tensile strength of line wires exposed to the atmosphere increases as the diameter of the wire is reduced [22]. This is because corrosion is a surface process, and

more surface sites exposed to the reactant result in higher corrosion rates.

5. Surface Heat Capacity

The heat capacity of a metal surface has an influence on the corrosion rate, but it is unclear whether this is due to the thickness of the metal itself, or to the heat capacity of other objects to which the metal is affixed. For example, if an unpainted aluminum-skinned aircraft is not maintained properly, corrosion is more pronounced on the underside of the wing because the underside of the wing has a low rate of heating and cooling. In the morning, the underwing remains cold longer than the rest of the aircraft, and retains condensation.

6. Metal Purity

It is generally true that the higher the degree of purity of aluminum, the greater its corrosion resistance. The corrosion resistance of aluminum declines appreciably as the purity drops from 99.998% to 99.98%. The decline is much less as the purity drops from 99.95% to 99.7% and still less as the purity drops from 99.7% to 99.0%. Obviously the nature of the impurities and the corrosive medium affects the extent of degradation caused by a given amount of contamination. These remarks apply to the impurities normally present in commercial metal. Certain elements such as Mg (noted above) increase the corrosion resistance.

7. Alloying Elements

The alloying elements used to fabricate most commercial aluminum alloys are: Major Alloying Elements: Cu, Mg, Mn Si, Zn; Minor Alloying Elements: Cr, Cu, Fe, Mn, Si, Ti. Those which increase the corrosion resistance of aluminum are: Cr, Mg, Mn. Those which decrease the corrosion resistance of aluminum are: Cu, Fe, Ni, Si, and Sn. Titanium appears to have little influence on corrosion resistance and is usually added to act as a grain refiner.

III. Experimental Procedures

A. Instrument Detail

Auger measurements were performed in a load-locked Kratos XSAM 800 surface analysis system equipped with a hemispherical energy analyzer. The base pressure of this ion- and turbo-pumped system is 1×10^{-10} torr as read on an uncalibrated, cold cathode gauge.

Auger spectra were excited by an electrostatically focused electron gun containing a LaB_6 thermionic emitter whose energy was variable from 0-10 keV. Objective, condenser, and stigmator lens voltages were varied by analog potentiometers to form a focused beam at an incident angle of 60° to the specimen normal. The sample working distance was 17 mm. Although scanning and video capabilities are available in this system, the Auger electronics were operated in the fixed-beam mode during the measurements. All Auger spectra were recorded at 5.0 keV beam energy and 1.0 μA primary beam current, measured with applied +90 V bias.

Ar^+ ion sputtering of the 2219 aluminum surfaces was accomplished by a differentially pumped Kratos Minibeam I plasma discharge ion source with rastering and focusing capabilities. The beam voltage of this gun was variable from 0-5 kV, regulated and resettable to 1%. The electron emission current was variable from 5 to 25 mA, and feedback regulation to 1% ensured high current stability during operation. Beam focus was controlled by adjustable voltages applied to the electrostatic lens elements in the gun. The beam diameter was roughly 0.1 mm at the sample working distance (25 mm). Both X- and Y-deflection was possible which allowed for precise DC positioning of the ion beam. A variable scan voltage provided a high frequency scan mode which permitted a sputtered area of 1 cm^2 at the specimen position. Auger spectra were taken in spot mode at a position near the center of the sputtered area. The angle of incidence of the ion beam with respect to the surface normal was 55°.

Auger spectra were collected by a Kratos Series 800, 127 mm radius double focusing concentric hemispherical energy analyzer (CHA) equipped with an aberration compensated input lens (ACIL). It is possible to select variable pass energies, retard ratios, and magnifications by computer control. Auger spectra were recorded in the fixed-retard ratio (FRR) mode with a retard ratio of 10.

Such a retard ratio represents a compromise between sensitivity and resolution and is appropriate for acquisition of survey spectra. The magnification of the analyzer in the FRR mode was selected to collect electrons from the smallest allowable (5 mm^2) area on the specimen (High Mag), obtained by optimizing the lens functions of the 6 adjustable lenses in the ACIL. The AES energy resolution for the slit combination (full open) used was measured to be 0.24% on clean copper.

The detection system of our XSAM 800 consists of a single channel multiplier and a fast response head amplifier. Detector output modes include direct pulse counting and current detection with voltage to frequency (V-F) conversion. Due to the large exciting currents used, all spectra were taken in current detection mode.

The electron micrographs were taken with a Cambridge Stereoscan 200 scanning electron microscope. This ion- and turbo-pumped instrument has a LaB_6 thermionic emitter with a maximum magnification of about 300,000 X. It has a 3 lens electron optical column with four selectable apertures, and an octapole stigmator with X- and Y-control. The maximum beam voltage is 30 kV, and it is equipped with both backscattered and X-ray detectors.

EDX spectra were obtained by an EGG Ortek Series 5000 energy dispersive wavelength spectrometer attached to the Cambridge SEM. This system possesses a liquid nitrogen cooled lithium-drifted silicon Si(Li) X-ray detector with a low-noise FET first stage which uses dynamic charge restoration. The detector resolution is 148 eV and is protected by a Be window. A software controlled A/D converter allows a wide variety of acquisition modes and data analysis. Elemental compositions were determined by the ZAP II program, which is discussed in Scanning Electron Microscopy, 1982, III, pp. 981-993. The program includes automatic background subtraction, peak overlap correction including escape peaks, detector efficiency correction, and relative atomic, absorption, and fluorescence corrections. It is insensitive to drifts in the microscope beam current.

B. The Corrosion Experiment

The experimental setup used to study aluminum corrosion is shown in Figure 1. A standard Pyrex beaker was filled with roughly 200 ml of Gulf Coast seawater, sealed with a rubber stopper, and placed atop a heater/stirrer table. A thermometer and specimen holder containing the 2219 aluminum sample protruded through the stopper. Temperatures were rigorously controlled during the experiment by varying the heater current, and the seawater was gently agitated during the exposure by the magnetic stirrer. The experimental matrix is shown in the diagram on the following page.

The Gulf Coast seawater was obtained near Destin, Florida. The water temperature on that day was measured to be 30 C (86 F), and its pH was measured to be 7.6 with a digital pH meter calibrated against standard solutions. The chemical composition of the seawater is not known. It is generally recognized, however, that while the salinity of seawater varies from place to place, the relative proportions of the major constituents are relatively independent of location. The average concentrations of the principal constituents were given previously in Table I. The average salinity of seawater is about 35 grams of dissolved salts per kilogram of seawater.

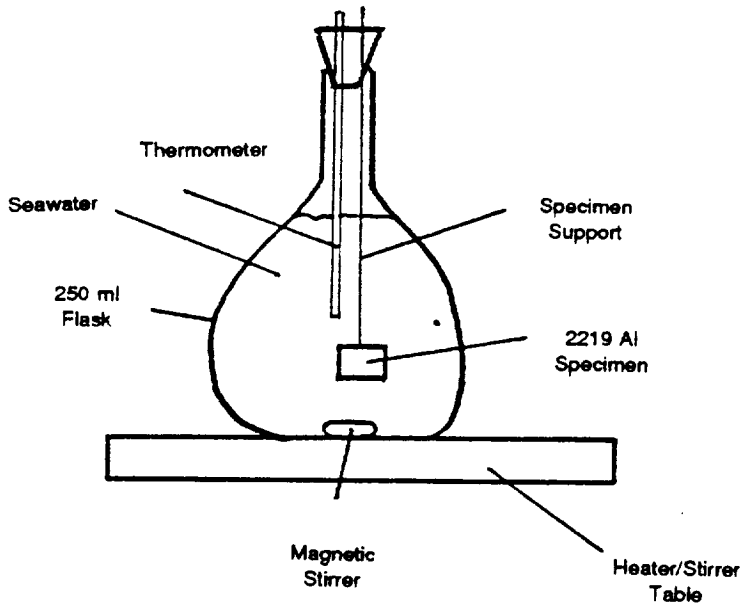

Fig. 1. Experimental apparatus used to study seawater corrosion.

Experimental Matrix

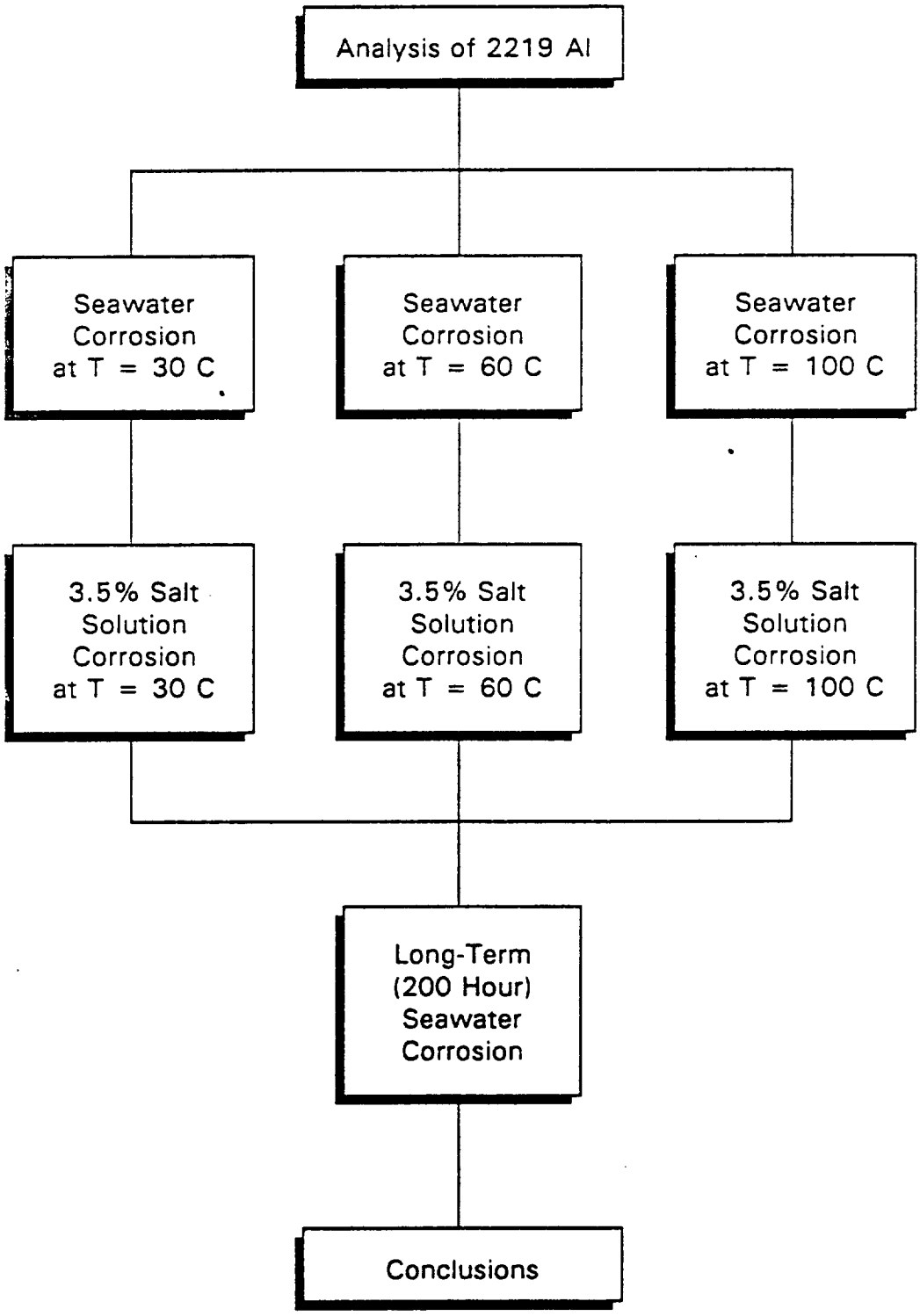

C. Materials and Sample Preparation

The 2219 Al-Cu alloy was supplied by Marshall Space Flight Center. Small sections (1 cm X 1 cm X 1 mm) were cut from stock 2219 material used in construction of NASA solid rocket booster assemblies. Roughly 20 pieces were supplied to AU. The 2219 pieces were ultrasonically cleaned in solutions of trichloroethylene, isopropyl alcohol, and DI water. The specimens were subsequently exposed to seawater or salt solution and then loaded directly into the Auger or SEM systems for analysis. The alloy surfaces were characterized both before and after exposure to the corrosive environment.

IV. The 2219 Al-Cu Alloy Before Exposure

Measurements were first made to identify the bulk and surface impurities inherent to the 2219 alloy material prior to seawater exposure, and to provide a baseline for the controlled exposure experiments. Methods used were SEM microstructural analysis, EDX (energy dispersive X-ray analysis), and Auger electron spectroscopy (AES).

A. Bulk / EDX Analysis

An SEM micrograph of as received 2219 aluminum is shown in Figure 2. The surface is uniformly pitted with 10-20 micron wide depressions which may serve as active sites for corrosion. An EDX spectrum indicating the bulk composition of 2219 aluminum is provided in Figure 3. The 2219 aluminum alloy has been described above; it is an Al-Cu alloy (86% Al, 5.8% Cu) with small percentages of Ar (6%), P(3%), and Mn (0.04%). The EDX derived composition is in qualitative accord with chemical composition data given in metals handbooks for 2219 aluminum (see Table II). The EDX technique with our current X-ray window cannot detect elements with $Z < 11$ (sodium). X-ray dot maps of Al and Cu showed no unusual microstructural features. The lateral distribution of Al and Cu is uniform throughout the 2219 alloy.

B. Surface / Auger Analysis

An Auger spectrum of the surface of as received 2219 aluminum is shown in Figure 4. The surface (defined as the top 30 Å of the aluminum) is primarily aluminum oxide, with small quantities of several elements: Si, S, Cl, K, C, Ca, N, F, Cu, Na, and Mg. Several of these elements are surface active (S, Na, Cl, K, Ca, F) and are characteristic of metal surfaces which have undergone extensive handling. The C and N signals are usually observed in Auger spectra of as received material and are due to atmospheric gas exposure. The Si appears to be a surface contaminant while Cu is part of the alloy composition. That the as received surface is aluminum oxide is shown by the i) lineshape and ii) energy of the Al (KLL) 1396 eV feature. This structure is distinctive of oxidized aluminum (see Figure 5). Compare the nonoxidized Al(KLL) feature in Figure 6. Since quantitation in Auger spectroscopy is poorly developed, we are unable to provide precise numbers for the amount of each surface contaminant present.

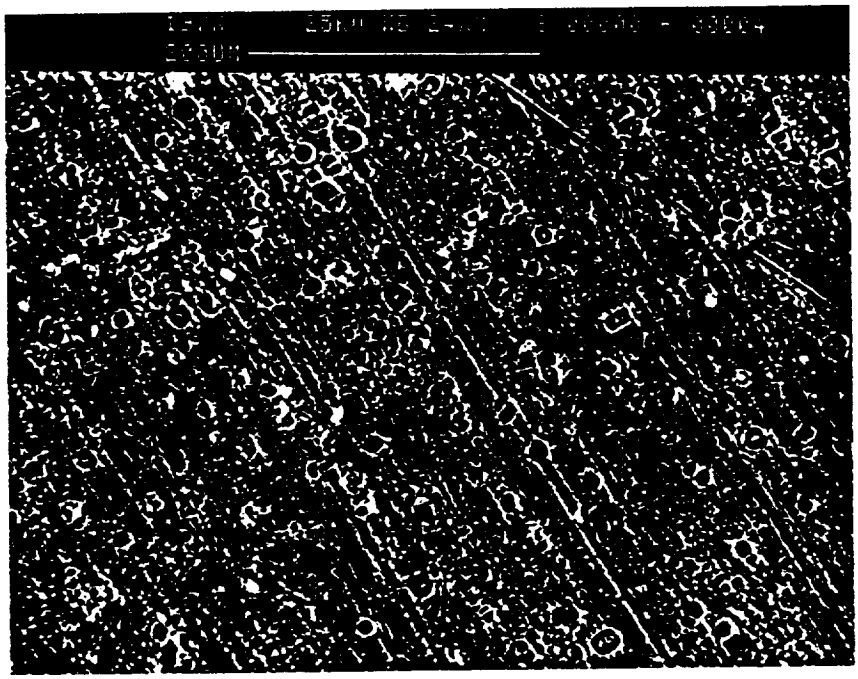

Fig. 2. SEM micrograph of as received 2219 aluminum used in SRB construction. The surface is uniformly pitted.

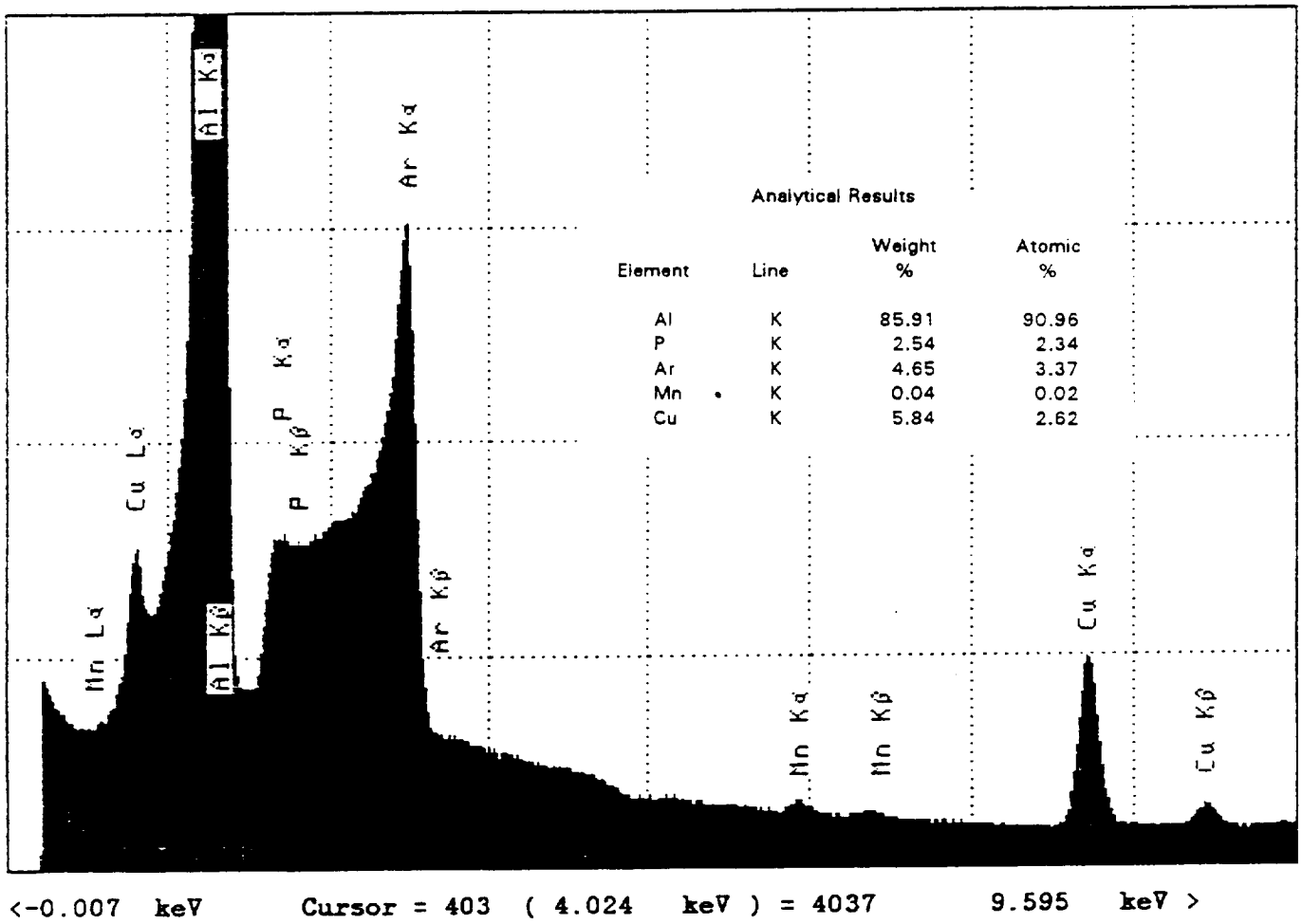

Fig. 3. EDX spectrum of as received 2219 aluminum used in SRB construction. The aluminum is an Al-Cu alloy composition with bulk contaminants of Ar, Mn, and P.

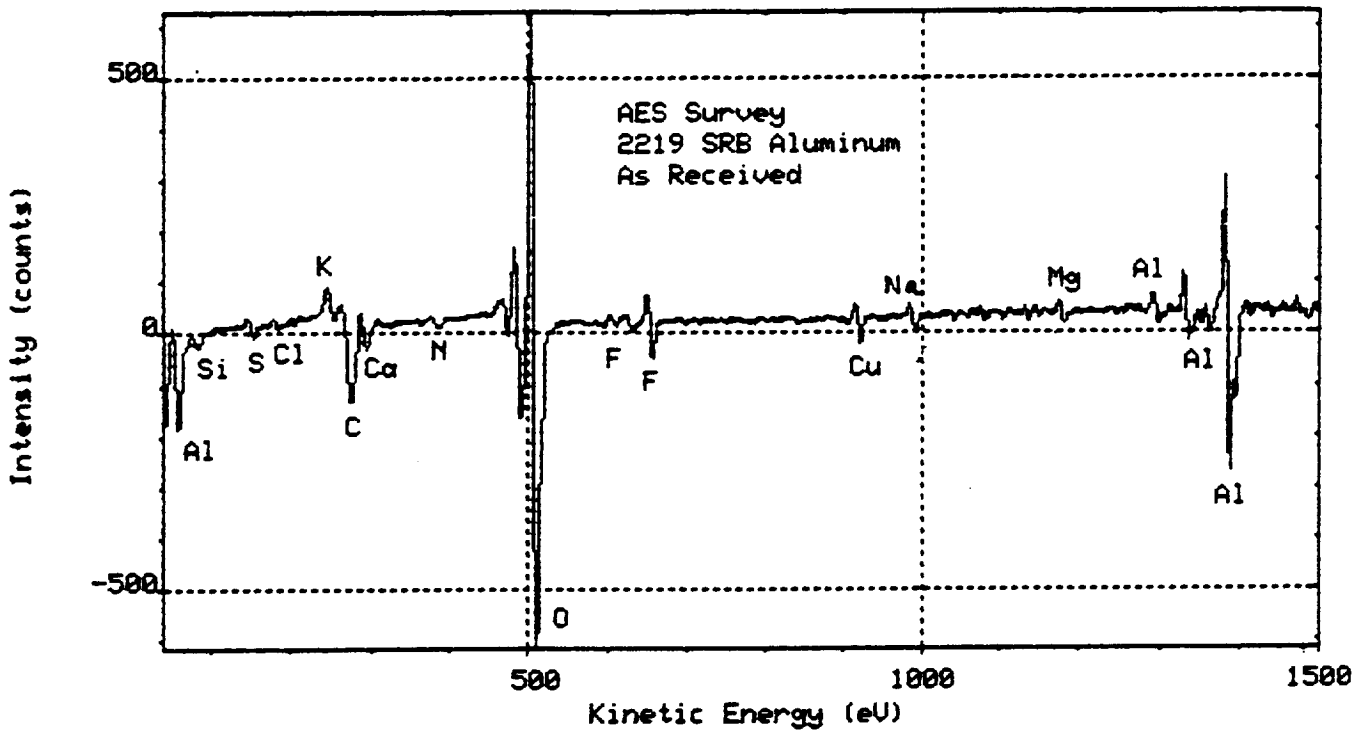

Fig. 4: Auger spectrum of as received 2219 aluminum used in SRB construction. The surface is oxidized with a number of contaminants present due to handling.

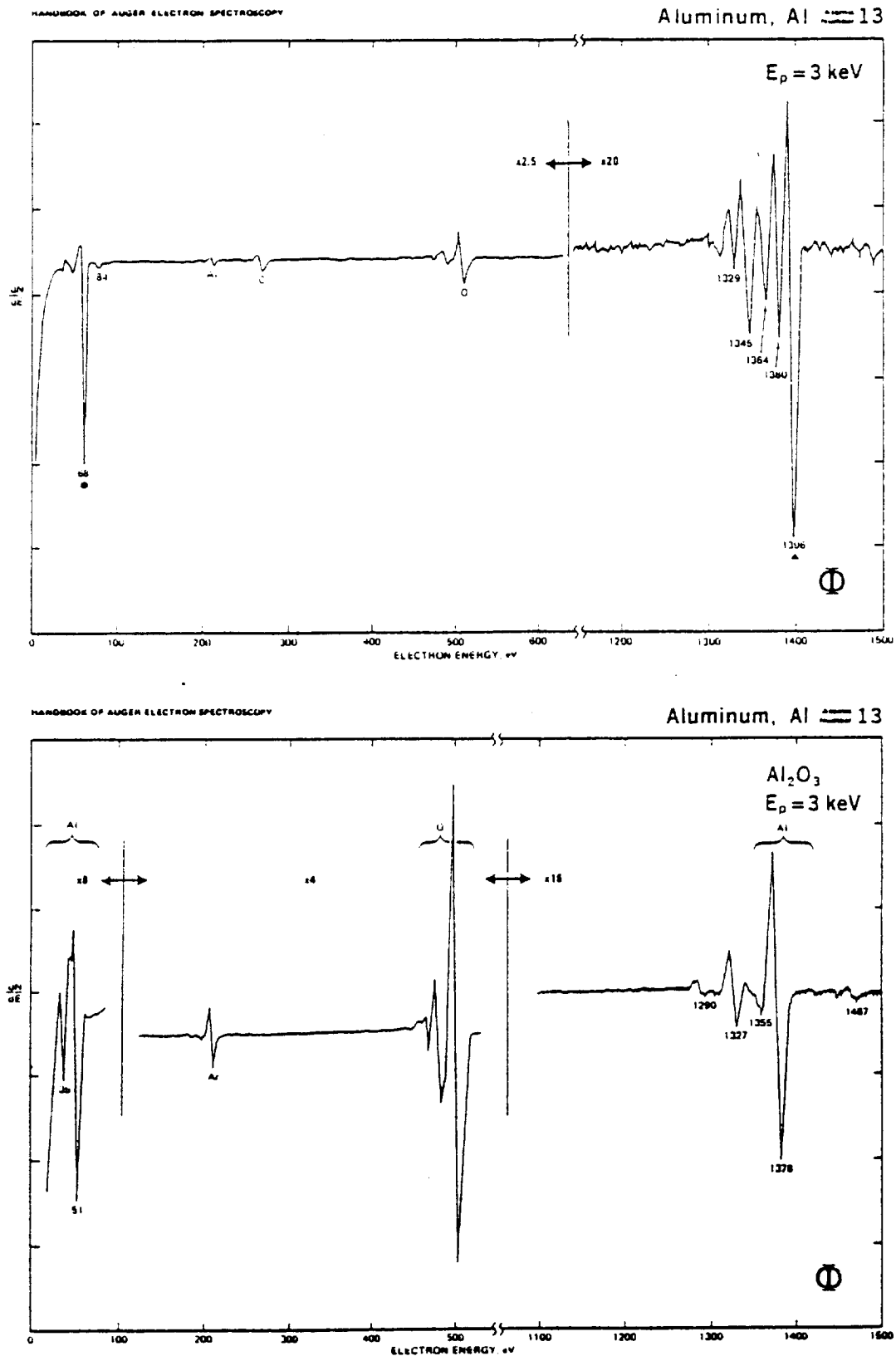

Fig. 5. Reference Auger spectrum of pure Al and stoichiometric Al_2O_3 [23].

Figure 6 shows the Auger spectrum of the 2219 aluminum surface after 8 minutes of Ar sputter cleaning. The Ar was supplied by an rastered ion gun operating at 3 kV energy. The sputter rate was 44 Å/min as measured on a standard of SiO_2. Assuming the sputter rates of SiO_2 and Al are equal, roughly 350 Å of the surface have been removed. The oxide layer and surface contaminants have been sputtered away and only signals from Al, O, C, and Ar are found. The Ar present is due to implantation from the ion gun, while the small amounts of C and O remaining appear to be incorporated into the aluminum (EDX cannot detect these elements). The Cu is part of the bulk alloy composition of 2219 aluminum, seen in EDX analysis. The Al(KLL) lineshape is characteristic of elemental aluminum (cf. Fig. 5). Careful sputtering studies showed the native oxide layer to be roughly 150 Å thick. After extensive sputtering (20-30 min), the Auger spectrum looked identical to that in Fig. 6, verifying the EDX results for the bulk composition. No other elements were observed within the detectability limit for Auger spectroscopy (0.1 % of a monolayer).

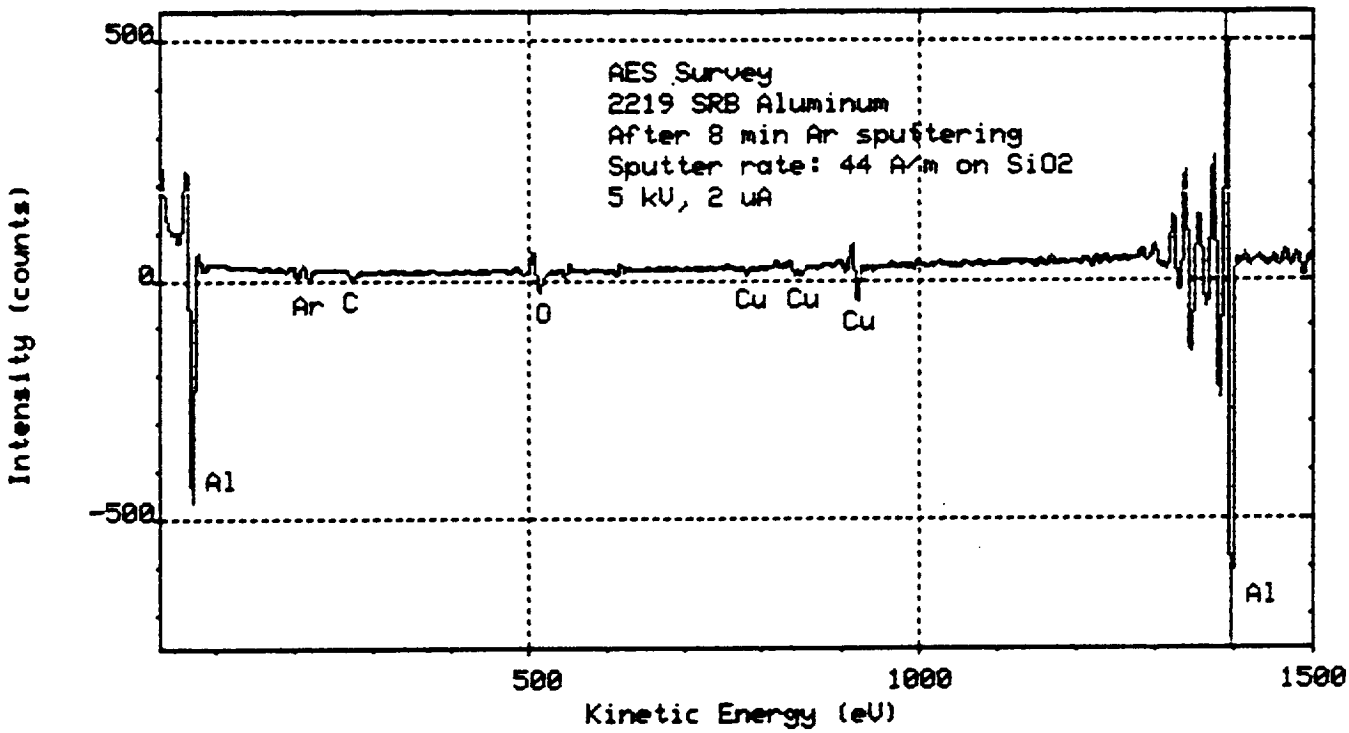

Fig. 6. Auger spectrum of 2219 aluminum after Ar sputter cleaning. The bulk alloy composition is reached after about 150 A of sputtering.

Table II

SRB 2219 Aluminum Bulk Composition
(wt %)

EDX Composition			Handbook Composition [a] (nominal)		
Al	-	85.9	Al	-	93.1
Cu	-	5.8	Cu	-	6.3
Ar	-	5.7	Ti	-	0.06
P	-	2.5	V	-	0.1
Mn	-	0.04	Mn	-	0.03
			Zr	-	0.18

[a]Metals Handbook, Volume 9, Metallography and Microstructures, 9th edition, p. 359

V. The 2219 Al-Cu Alloy Exposed to Seawater

A. Seawater Exposure at T = 30 C

An optical micrograph of the 2219 aluminum alloy before and after 2.0 hours of seawater exposure at T = 30 C is shown in Figure 7. The temperature of T = 30 C was chosen because it is roughly the temperature of Gulf seawater. The corrosion is extensive. Visible (dull grey) discoloration of the aluminum could be seen after 30 minutes of exposure, and at the same time, bubbles developed over localized portions of the aluminum surface. Optical and SEM microscopy (see Fig. 7(b)) shows that the surface is covered by corrosion products in the form of discrete, localized mounds of second phase material. A closer view is shown in Figure 8. Figure 8(a) is a high magnification optical photograph of the corrosion products on the lower right-hand side of Fig. 7(b). Figure 8(b) is an SEM micrograph of one of the localized mounds.

EDX analysis of one of the crystalline mounds (position 1 in Fig. 8(b)) is shown in Figure 9. The mound is mostly Al, S, Na, and Cl with small (<2%) percentages of K, Ca, Cr, Mn, Fe, Ni, and Cu. It is questionable how much of the Al signal originates from the mound and how much originates from the Al substrate. This is because it the thickness of the material is unknown. The incident electron beam penetrates roughly 1 micron of material per every 10 kV of accelerating voltage, and since the analysis was carried out at 25 kV, this means that the majority of X-rays originate from material located a couple of microns under the surface. Further, it is possible to have substantial electron scattering when performing EDX analysis on rough, irregular features. The scattered electrons can excite X-rays in nearby (substrate) material and give the impression that more aluminum is in the analysis feature than is real. Auger analytical results discussed below resolves this situation.

EDX analysis of the exposed aluminum surface away from the corrosion mounds is shown in Figure 10. The composition is nearly identical to the unexposed bulk alloy composition. It is likely that reaction products are present, but reside in a thin surface layer that are missed by the deep penetration of the incident electron beam. This is indeed the case, shown by Auger analysis.

(a)

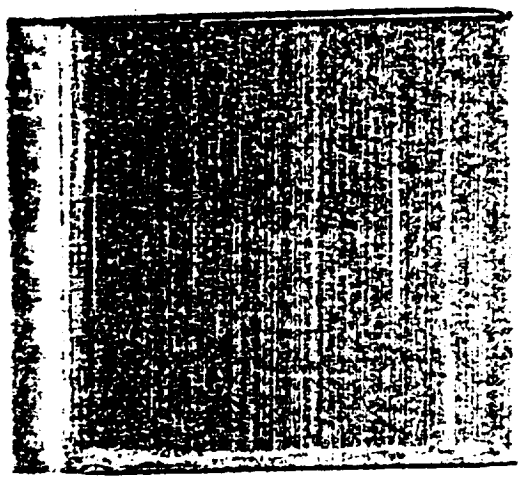

(b)

Fig. 7. Optical micrographs of 2219 aluminum (a) before and (b) after 2.0 hours of seawater exposure at T = 30 C.

(a)

(b)

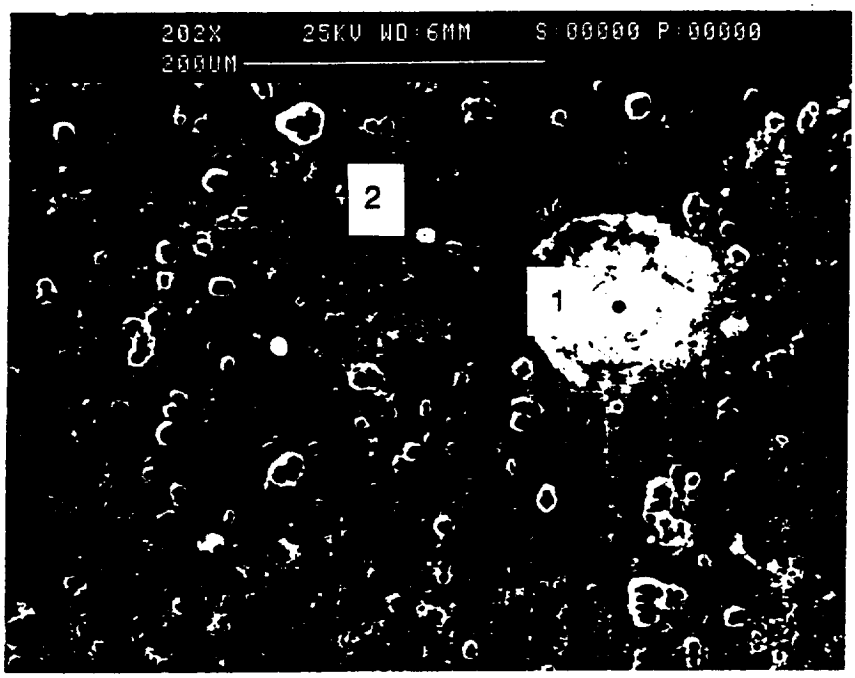

Fig. 8. High magnification (a) optical and (b) SEM views of the T = 30 C corrosion products.

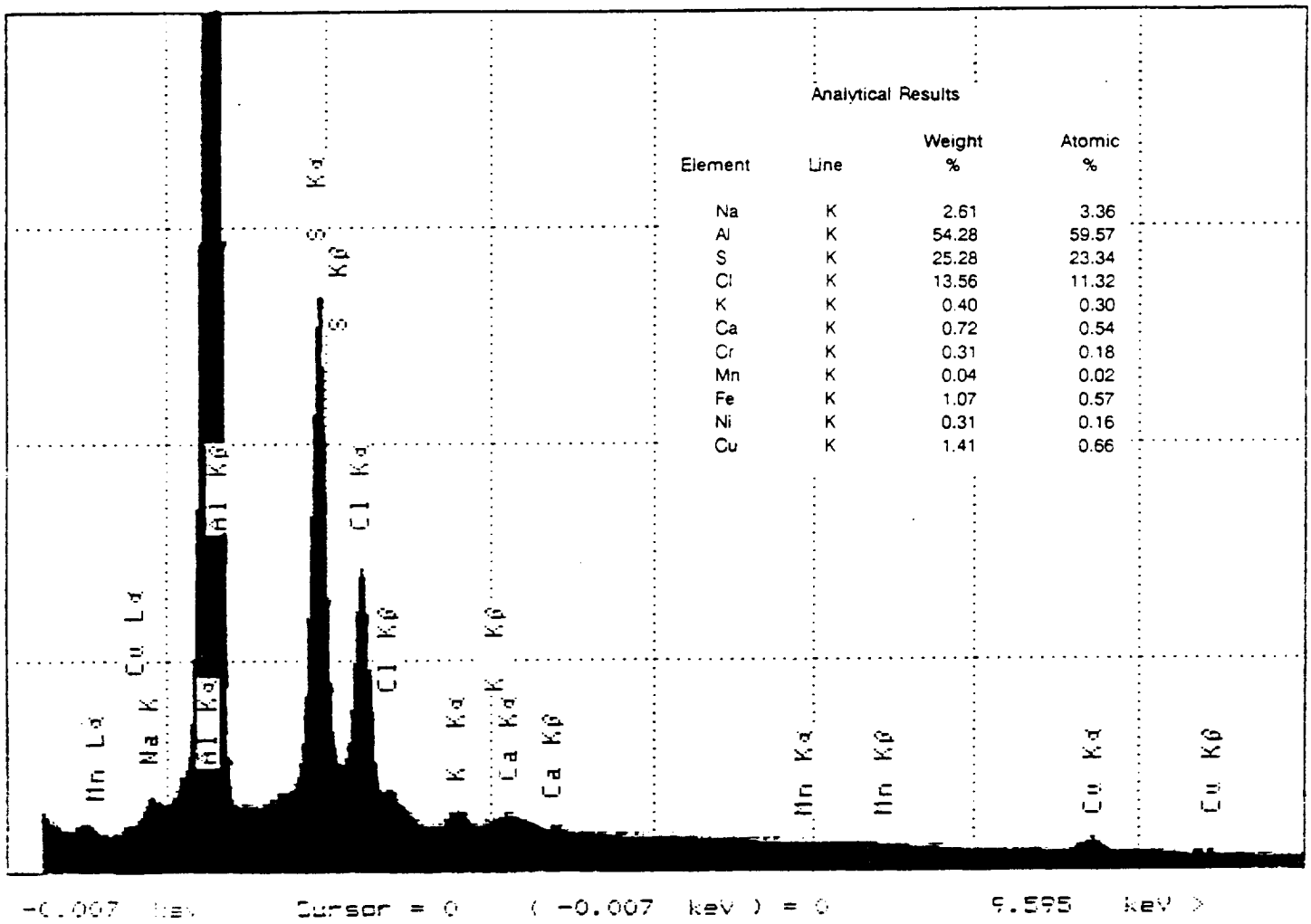

Fig. 9. EDX spectrum atop a localized mound of second phase material (position 1 in Fig. 8(b). The major elemental constituents are Al, S, Na, and Cl. The EDX technique with our current X-ray window cannot detect elements with atomic number Z < 11 (Na).

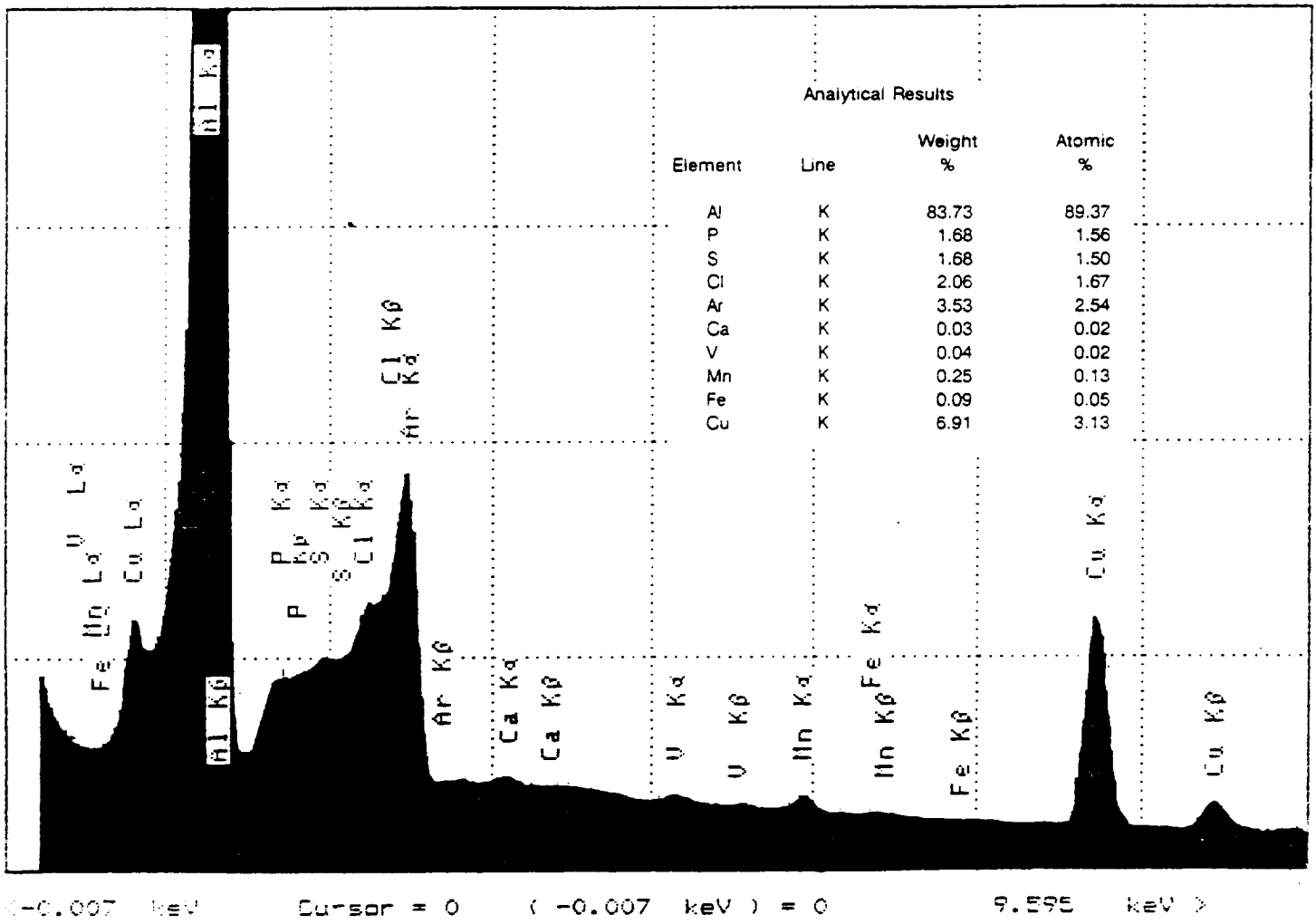

Fig. 10. EDX spectrum of the 2219 aluminum surface away from a corrosion mound (position 2 in Fig. 8(b). The composition reflects the bulk alloy composition with the addition of small quantities of S, Cl, Ca, V, and Fe.

That much of the Al signal seen in EDX analysis originates from the corrosion mounds rather than the 2219 substrate itself was found during Auger analysis of the corrosion surface. If fact, Auger analysis makes it clear that Al is present in the mounds in the form of aluminum oxide (Al_2O_3). Auger analysis atop the localized mound (position 1 in Fig. 8) is shown in Figure 11(a). The Auger signature is clearly that of Al_2O_3, shown both by the energies and shapes of the Al Auger peaks. Auger analysis off to the side of the mound (position 2 in Fig. 8) is nearly identical to the Auger spectrum on the mound, with the addition of Mg. We attempted to determine how thick the mound of Al_2O_3 was by sputter etching through it. Based upon a sputter rate of 70 Å/m on SiO_2 (a common calibration material), it took roughly 4.5 hours to drill through the mound, corresponding to a thickness of ~1.9 microns. Since the spectroscopic information from EDX originates from roughly the top 2-3 microns of the surface, most of the elements found in earlier EDX spectra on localized mounds originate from the mounds themselves rather than from the 2219 substrate.

The specimen weight and size and the pH of the seawater was carefully measured before and after the corrosion experiment. There was no measurable difference in the size of the 2219 specimen, but the weight increased from 0.26870 g before exposure to 0.26875 g after exposure, reflecting the precipitated aluminum oxide. The pH of the seawater also increased, from 7.6 (before) to 7.8 (after), reflecting a decrease in $[H^+]$.

A puzzling feature of the Auger results is the relative absence of Na and Cl in the spectra. This appears to be true despite EDX analysis which showed substantial concentrations of these elements on the reacted surfaces. What happened to the Na and Cl?

The Na and Cl are indeed part of the reaction products, but these elements are difficult to observe in Auger spectroscopy due to the phenomenon of electron stimulated desorption (ESD). ESD is commonly observed in electron spectroscopy on fluorinated and clorinated surfaces. It makes detection of Cl, F, etc. difficult because Cl present on the surface desorbs from the surface (due to the interaction with the probing electron beam) before it can be detected.

ESD effects on seawater exposed 2219 surfaces is observed in Figure 12. This figure shows an Auger spectrum from the T = 100 C surface (discussed ahead; cited here for illustrative purposes only) which EDX analysis showed to

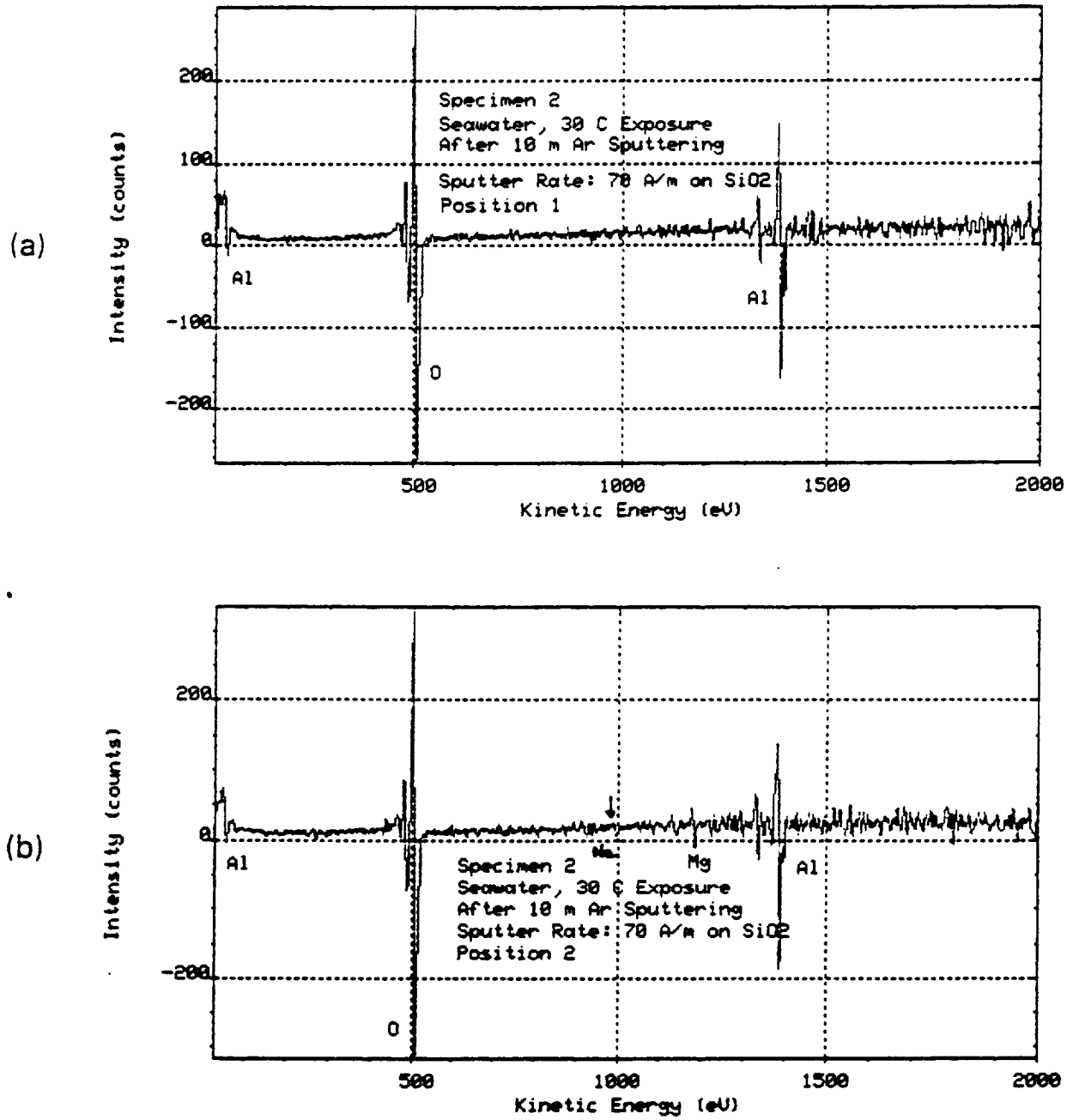

Fig. 11. Auger spectra (a) atop and (b) beside the localized mound in Figure 8 (see positions 1 and 2 in Fig. 8). The signatures are those of Al_2O_3 and MgO. The mounds appear to be primarily Al_2O_3 while the adjacent areas are both Al_2O_3 and MgO. The specimens were Ar sputtered for 10 minutes beforehand to remove traces of adsorbed residual atmospheric gases.

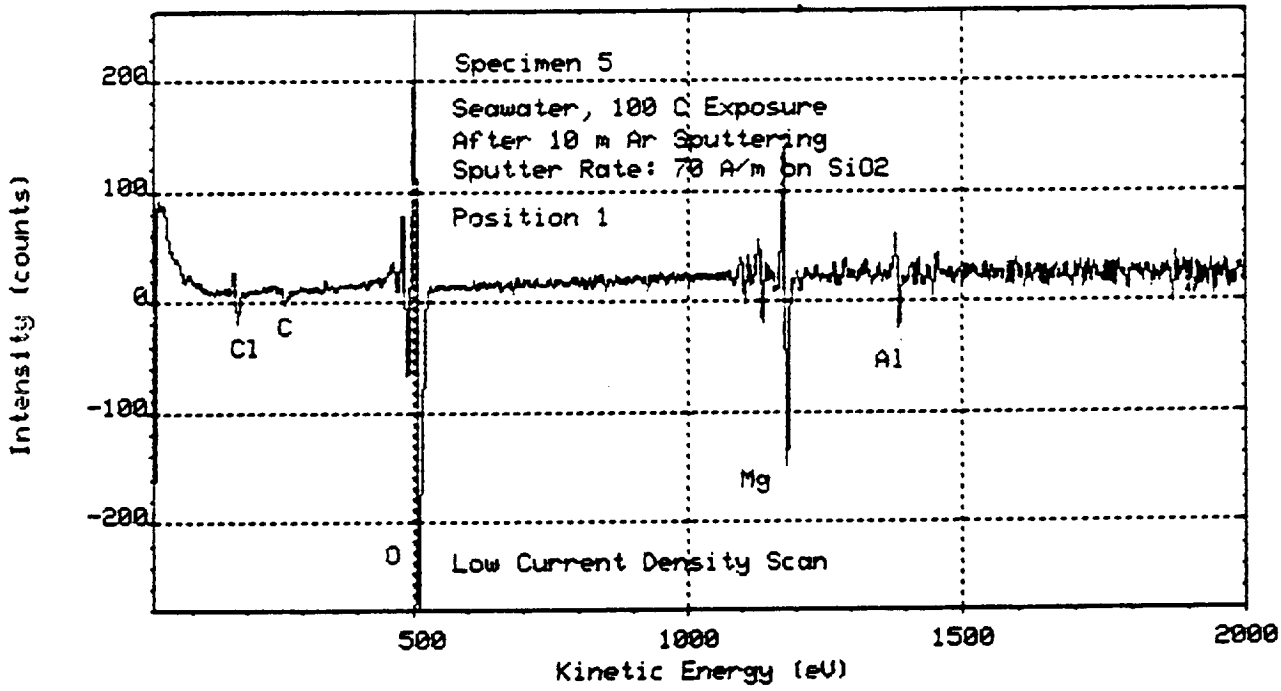

Fig. 12. A low current density Auger spectrum atop the T = 100 C reaction surface (cf. Fig. 24 for a high current scan), illustrating the effects of electron stimulated desorption on Auger spectra. Lower current densities result in reduced Cl desorption and a larger Cl peak.

contain substantial Cl, but at low voltage and current density which minimizes the effects of ESD. The Cl signal is clearly evident. Further evidence of ESD phenomenon involves the diminution of the Cl Auger feature with scan time. The magnitude of the Cl Auger peak diminishes significantly with scan time. By the time the S/N is sufficient in most spectra, the Cl has all desorbed. The moral is clear: both EDX and AES are necessary for complete analysis of surfaces exposed to seawater (chlorinated) solutions. Since most of the EDX signal originates from beneath the surface, the effects of ESD in EDX spectroscopy are minimal. The limitation of EDX, however, is that it cannot detect elements with $Z < 11$ (Na) with our current X-ray window.

B. Seawater Exposure at T = 60 C

At higher temperature, the corrosion is similar to that observed at T = 30 C (mounds are still observed) but with: i) increased growth of cubic crystals on the surface; ii) raised metallic areas that are lifting away from the Al surface. An optical micrograph of the 2219 aluminum alloy before and after 2.0 hours of seawater exposure at T = 60 C is shown in Figure 13. Visible (dull grey) discoloration of the aluminum could be seen after about 15 minutes of exposure, and at the same time, bubbles developed over much of the aluminum surface. Figure 13(b) shows that the corrosion products consist of localized, circular mounds of growing second phase material in addition to a uniform film of crystalline material covering the surface. The lifted areas could only be viewed by stereo microscopy and are not shown. The (lighter) square areas near the center of the specimen are where the electron beam rastered over the surface before seawater exposure. Apparently, the surface/electron beam interaction has altered the aluminum's corrosion characteristics.

High magnification SEM views after seawater exposure at T = 60 C are shown in Figures 14 and 16. Figure 14 shows two areas of the surface where growth of cubic crystalline material is extensive. An EDX spectrum atop one of the cubic structures (position 1 in Fig. 14(a)) is displayed in Figure 15. The crystal is composed primarily of Al, Na, and Cl. It is clear that the cubic crystals are NaCl and it is likely that the corrosion of the Al is catalyzed by the salt and sulphate ions in seawater, similar to rust developing on a car in wintertime when exposed to salt on an icy roadway.

(a)

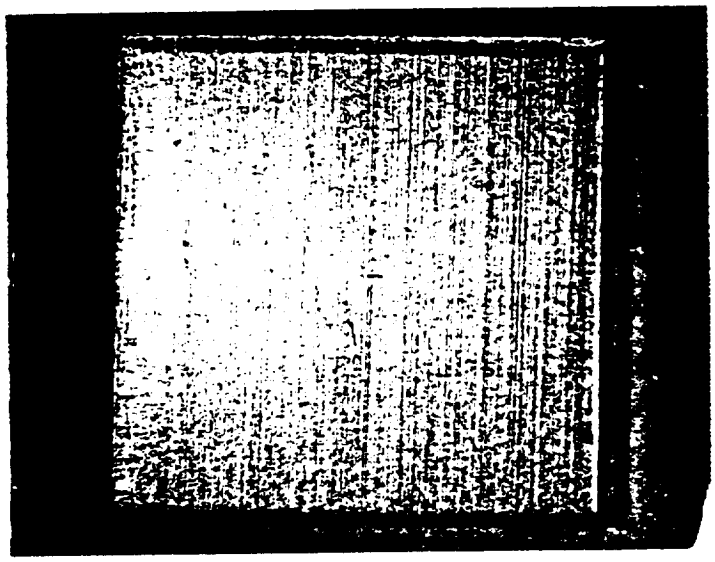

(b)

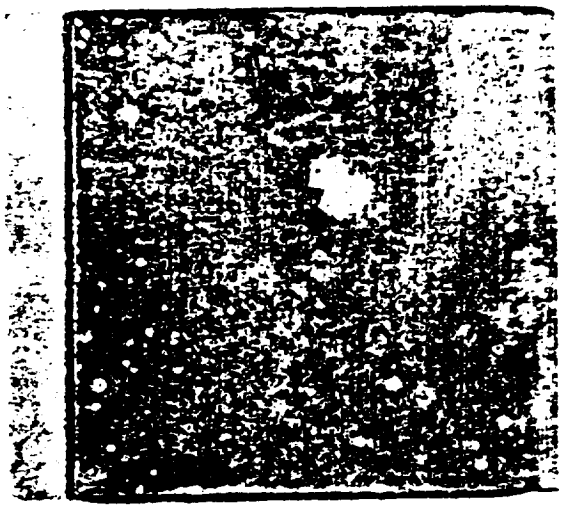

Fig. 13. Optical micrographs of 2219 aluminum (a) before and (b) after 2.0 hours of seawater exposure at T = 60 C.

(a)

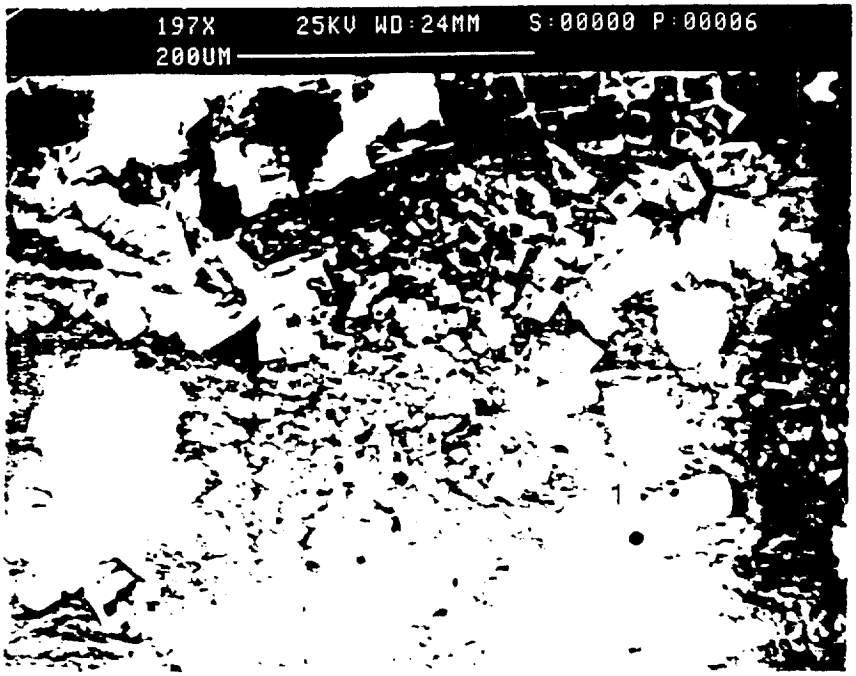

(b)

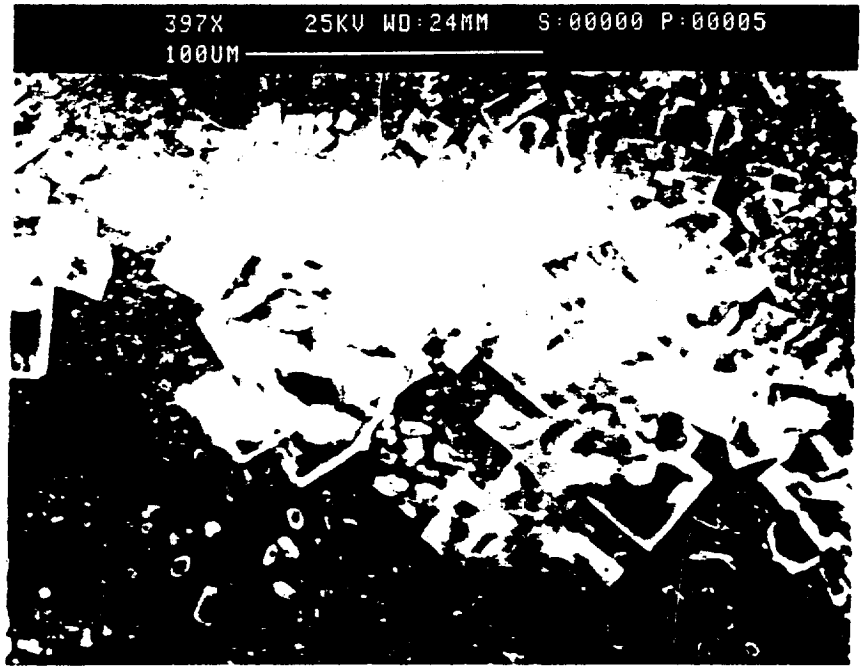

Fig. 14. High magnification SEM views of the T = 60 C corrosion products, in a region where extensive growth of cubic crystals occurred.

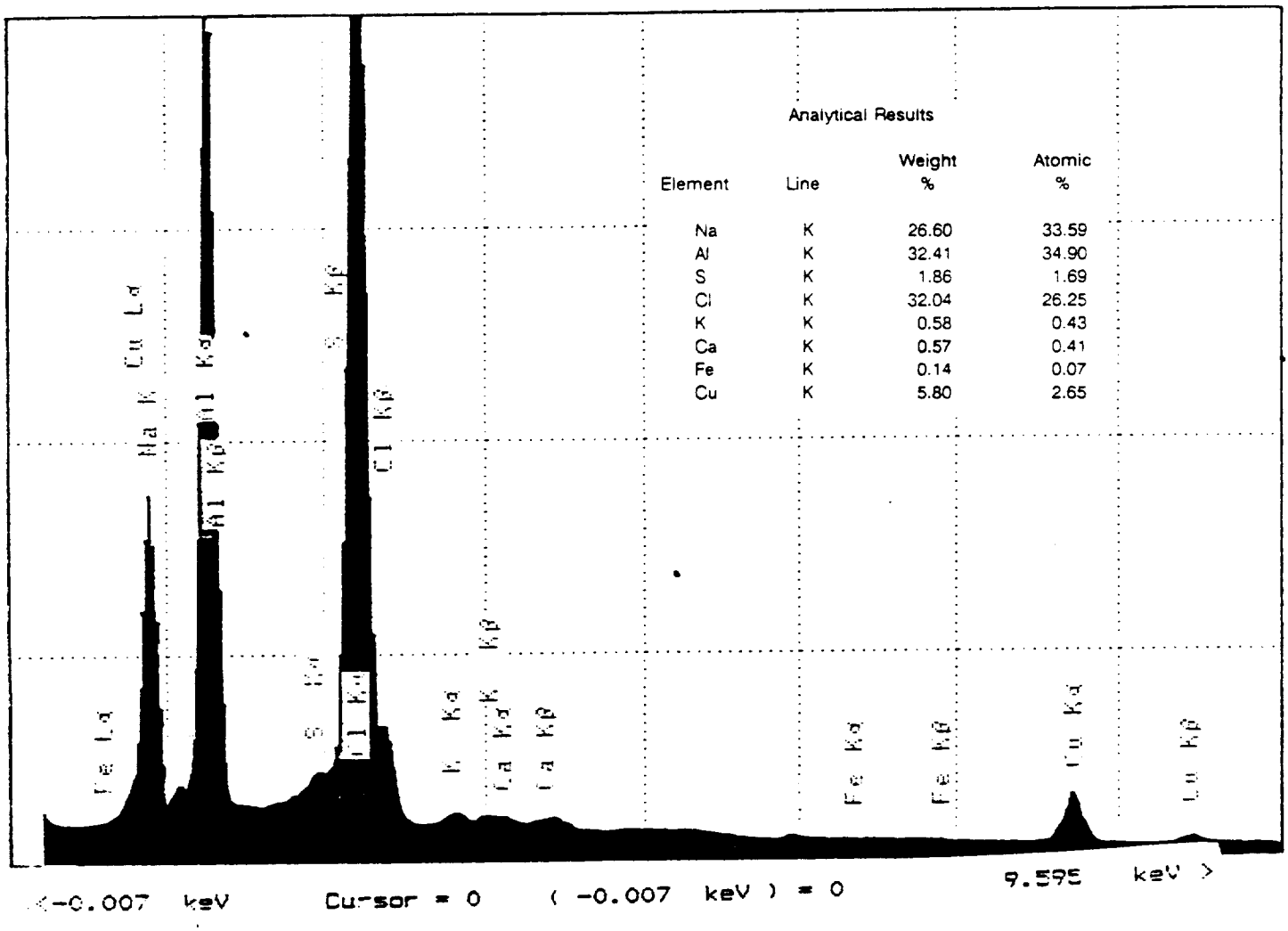

Fig. 15. EDX spectrum atop one of the cubic structures (position 1 in Fig. 14). The major elemental constituents are Al, Na, and Cl.

Figure 16 shows another section of the corroded surface showing a closeup of the small localized moundlike structures. The center of the micrograph shows growth structures consisting of several small cubes with four branching dendrites extending from each corner. The catalytic ability of this surface to form such structures is interesting.

Auger analysis atop one of the localized mounds (position 1 in Fig. 14(b)) is shown in Figure 17(a). The signature is clearly that of Al_2O_3, shown by both the energies and shapes of the Al Auger peaks. Auger analysis off to the side of the mound (position 2 in Fig. 14(b)) is nearly identical to the Auger spectrum on the mound, with the addition of Mg. The signature is clearly that of MgO, shown by the shape of the Mg Auger peak (see Figure 18). These results are similar to the case of T = 30 C seawater exposure, except with more MgO growth. Both surfaces are covered with Al_2O_3, NaCl, and MgO.

The specimen weight and size and the pH of the seawater was carefully measured before and after the corrosion experiment. There was no measurable difference in the size of the 2219 specimen, but the weight again increased from 0.26090 g before exposure to 0.26132 g after exposure, reflecting the precipitated second phase material on the aluminum. The pH of the seawater also increased, from 7.6 (before) to 7.8 (after). This was similar to the T = 30 C exposure case.

C. Seawater Exposure at T = 100 C

A specimen of 2219 aluminum was then placed into boiling seawater for a period of 2 hours. Visible (grey) discoloration of the aluminum was evident after minutes. The percolating seawater at the boiling point prevented bubbles (which were observed at T = 30 C and T = 60 C) from developing over the surface. Optical and SEM microscopy shows that the surface is covered by crystalline material which is less cubic in appearance than the case for T = 30 C and T = 60 C exposures. An optical micrograph of the 2219 Al alloy after seawater exposure is shown in Figure 19. The backside corrosion is shown in Figure 20. Figure 21 is an SEM micrograph of the backside corrosion products in an area where the most extensive crystal growth occurred.

(a)

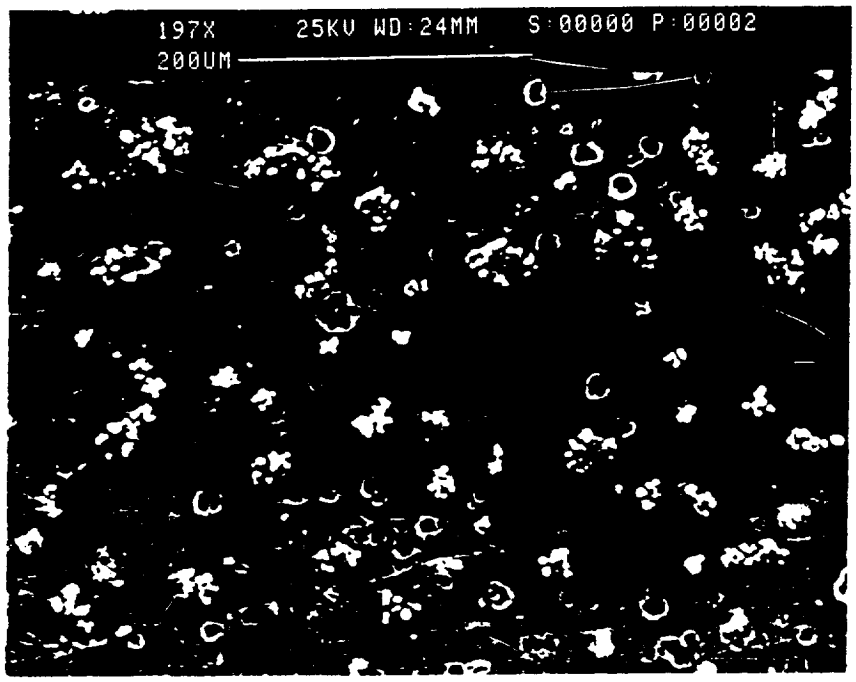

(b)

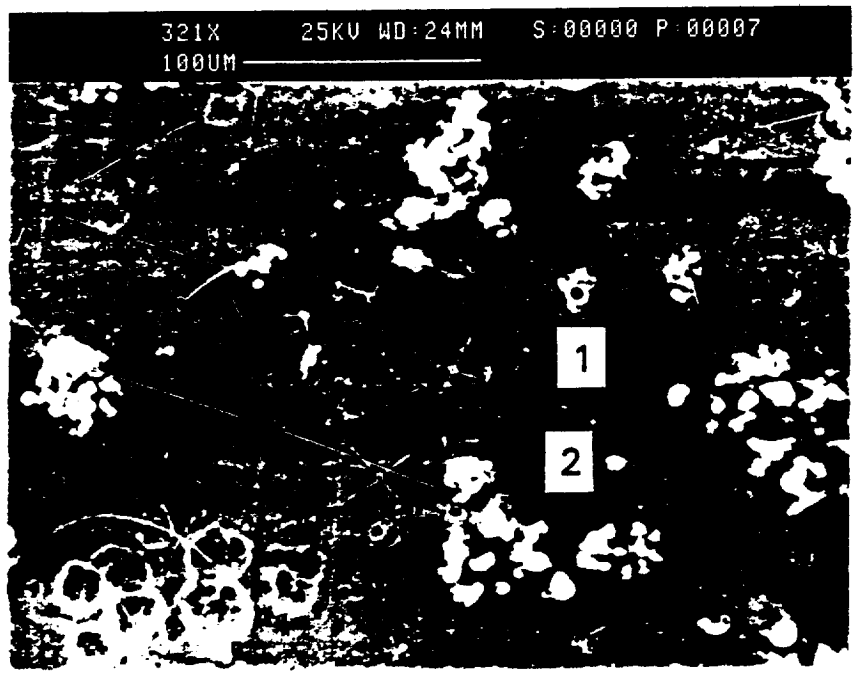

Fig. 16. High magnification SEM views of the T = 60 C corrosion products, in a region where small, localized moundlike structures are observed. The growth of small cubic crystals is also observed, with four dendrites extending from each corner.

(a)

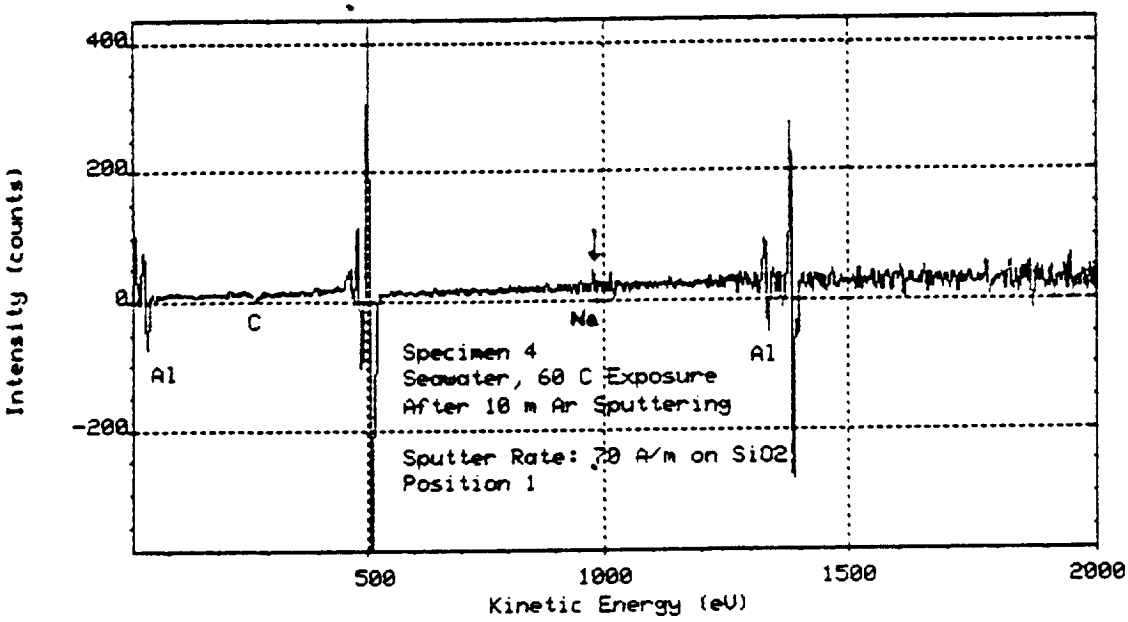

(b)

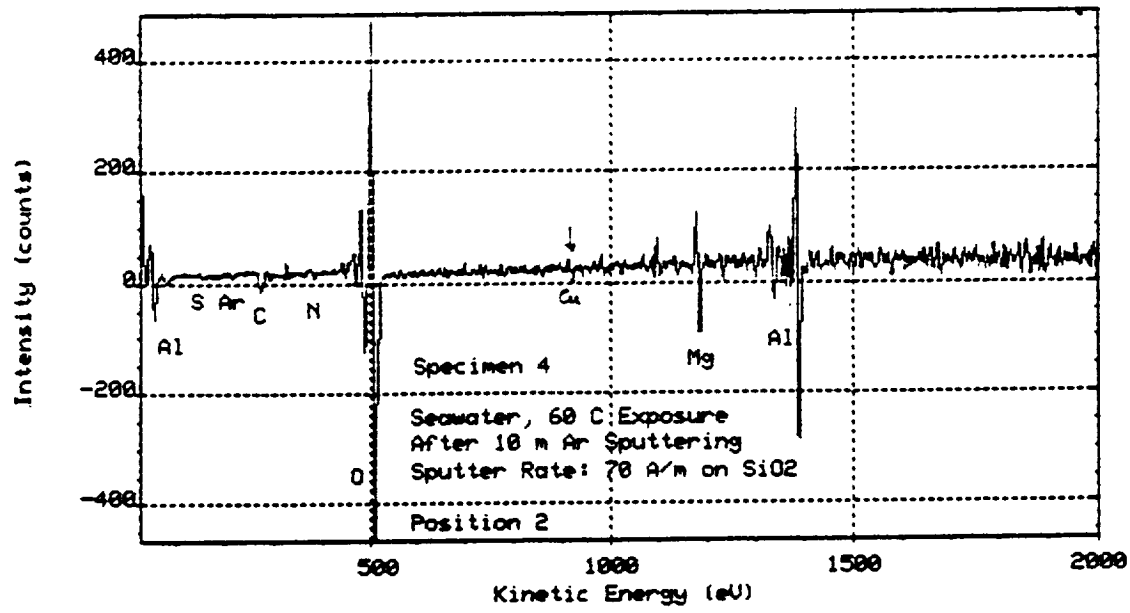

Fig. 17. Auger spectra (a) atop and (b) beside one of the localized mounds in Figure 16 (see positions 1 and 2 in Fig. 16). The mounds appear to be primarily Al_2O_3 while the adjacent areas are both Al_2O_3 and MgO. Exposure at higher temperature favors formation of MgO. The specimens were Ar sputtered for 10 minutes beforehand to remove traces of adsorbed residual atmospheric gases.

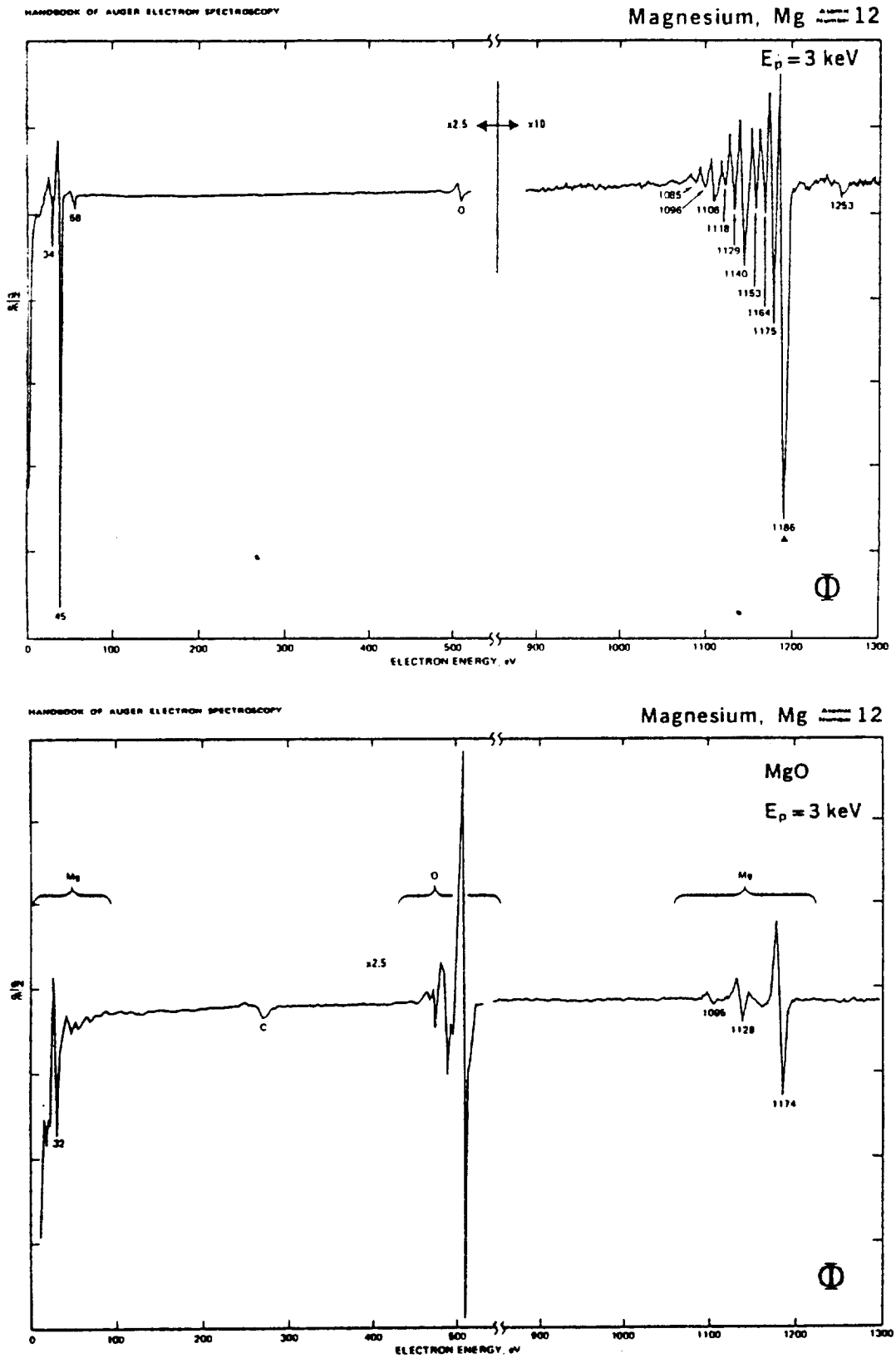

Fig. 18. Reference Auger spectrum for pure Mg and stoichiometric MgO [23].

(a)

(b)

Fig. 19. Optical micrographs of 2219 aluminum (frontside) after 2.0 hours of seawater exposure at T = 100 C. The view in (b) was taken at the lower left side of the view in (a). Extensive growth of crystalline material is evident, and a crystalline stringer is growing away from the surface.

(a)

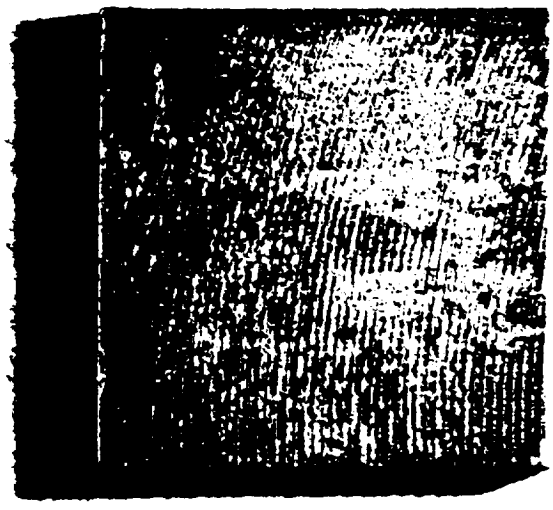

(b)

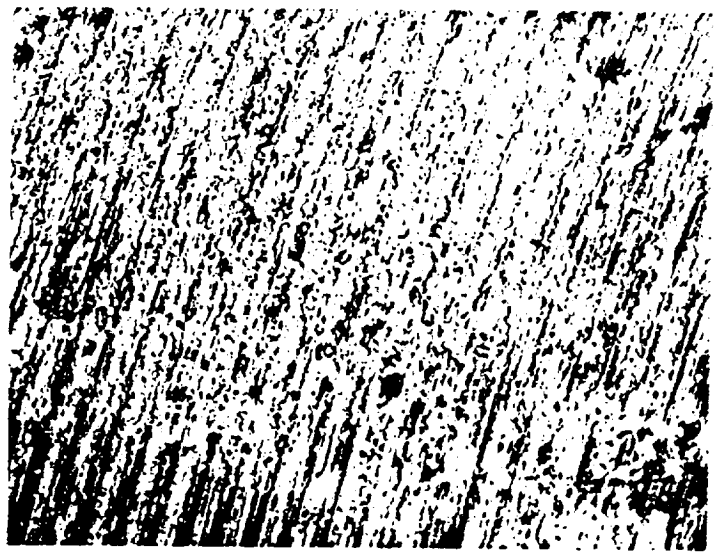

Fig. 20. Optical micrographs of 2219 aluminum (backside) after 2.0 hours of seawater exposure at T = 100 C. The view in (b) is a blowup of the corrosion products.

(a)

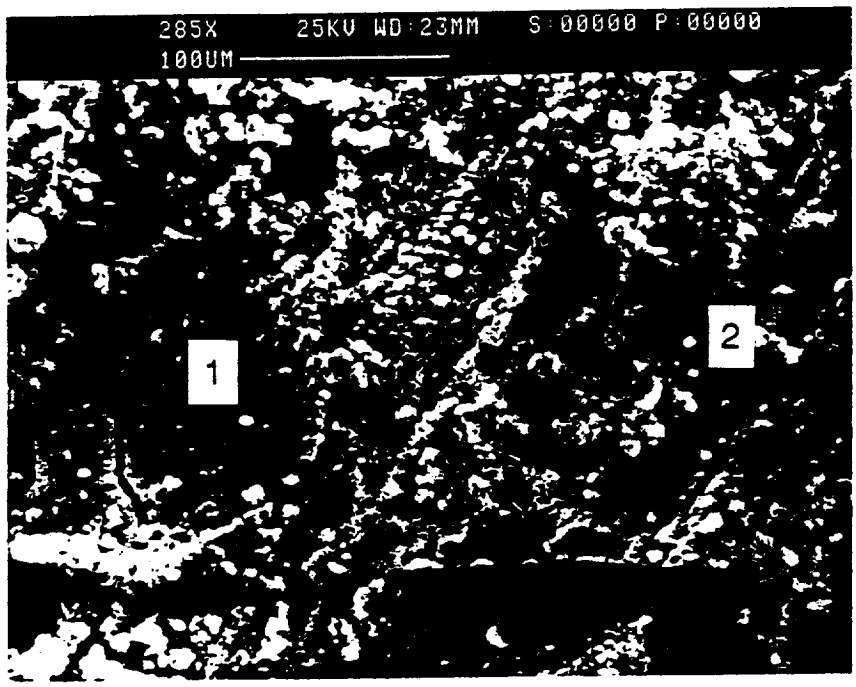

(b)

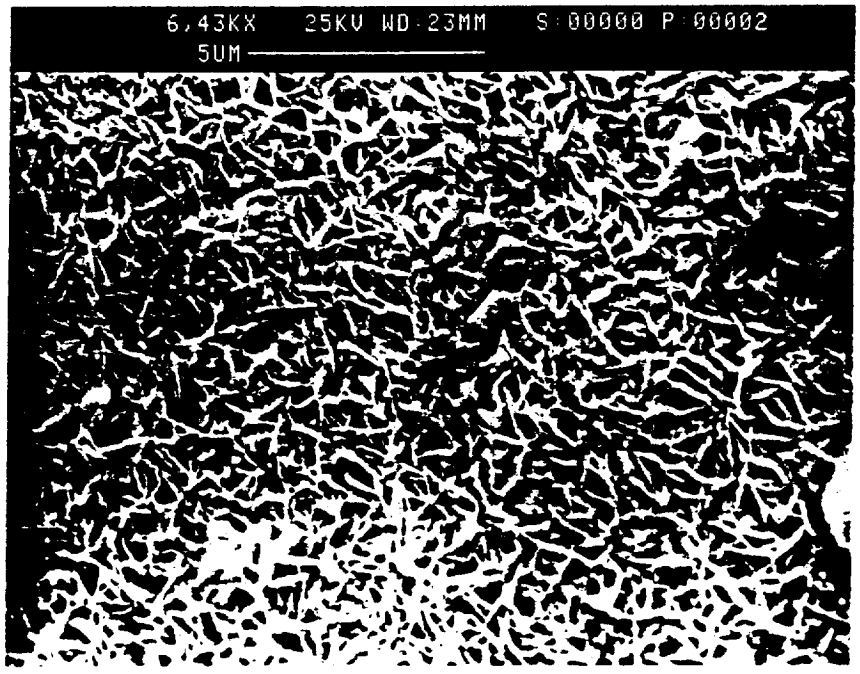

Fig. 21. High magnification SEM views of the T = 100 C corrosion products in a region where extensive crystal growth occurred. The view in (b) is a blowup of the region at position 1 in photo (a). The corrosion products are different in appearance (cf. Fig. 16) from the corrosion products observed at T = 60 C.

EDX analysis of two positions on the 2219 surface (positions 1 and 2 in Fig. 21(b)) is shown in Figures 22 and 23. The compositions are very similar at both locations, consisting primarily of Al, Mg, and Cl with small percentages of S, Si, Cu, Ca, Mn, and K. What is surprising about the analysis is that no Na is observed. Na was a major component of the crystalline material for the lower temperature (T = 30 C and T = 60 C) seawater exposures. In fact, no Mg was found in those instances. It appears that, despite its lower concentration in seawater (see Table I), the Mg^{+2} ion in seawater becomes a major player in the chemical reaction at high temperatures, while the role of Na^{+} is dominant at lower temperatures.

Auger analysis atop the corrosion products is shown in Figure 24. The signature again shows Al_2O_3, seen by both the energies and shapes of the Al Auger peaks. However, in the T = 100 C exposure, an even larger peak of Mg is observed, also seen in EDX analysis. The signature is clearly that of MgO. The surfaces phases present after T = 100 C seawater exposure are therefore stoichiometric MgO, Al_2O_3, and perhaps some NaCl, although clearly the growth of MgO is favored at higher temperatures.

The specimen weight and size and the pH of the seawater was carefully measured before and after the corrosion experiment. There was no measurable difference in the size of the 2219 specimen, but the weight increased from 0.26276 g before exposure to 0.26346 g after exposure, reflecting the precipitated second phase material on the aluminum. The pH of the seawater also increased, from 7.6 (before) to 8.6 (after), reflecting a decrease in $[H^{+}]$.

D. Seawater Exposure Summary

SRB 2219 aluminum displays extensive formation of corrosion products after only two hours of seawater exposure at temperatures T = 30 C and T = 60 C. At the lower temperature (T = 30 C), the corrosion consists of localized mounds of Al_2O_3 and NaCl. At higher temperature (T = 60 C), much of the surface is covered with NaCl and several areas of the alloy are beginning to lift away from the surface. At T = 100 C, the presence of both Al_2O_3 and MgO are observed, but growth of MgO is favored.

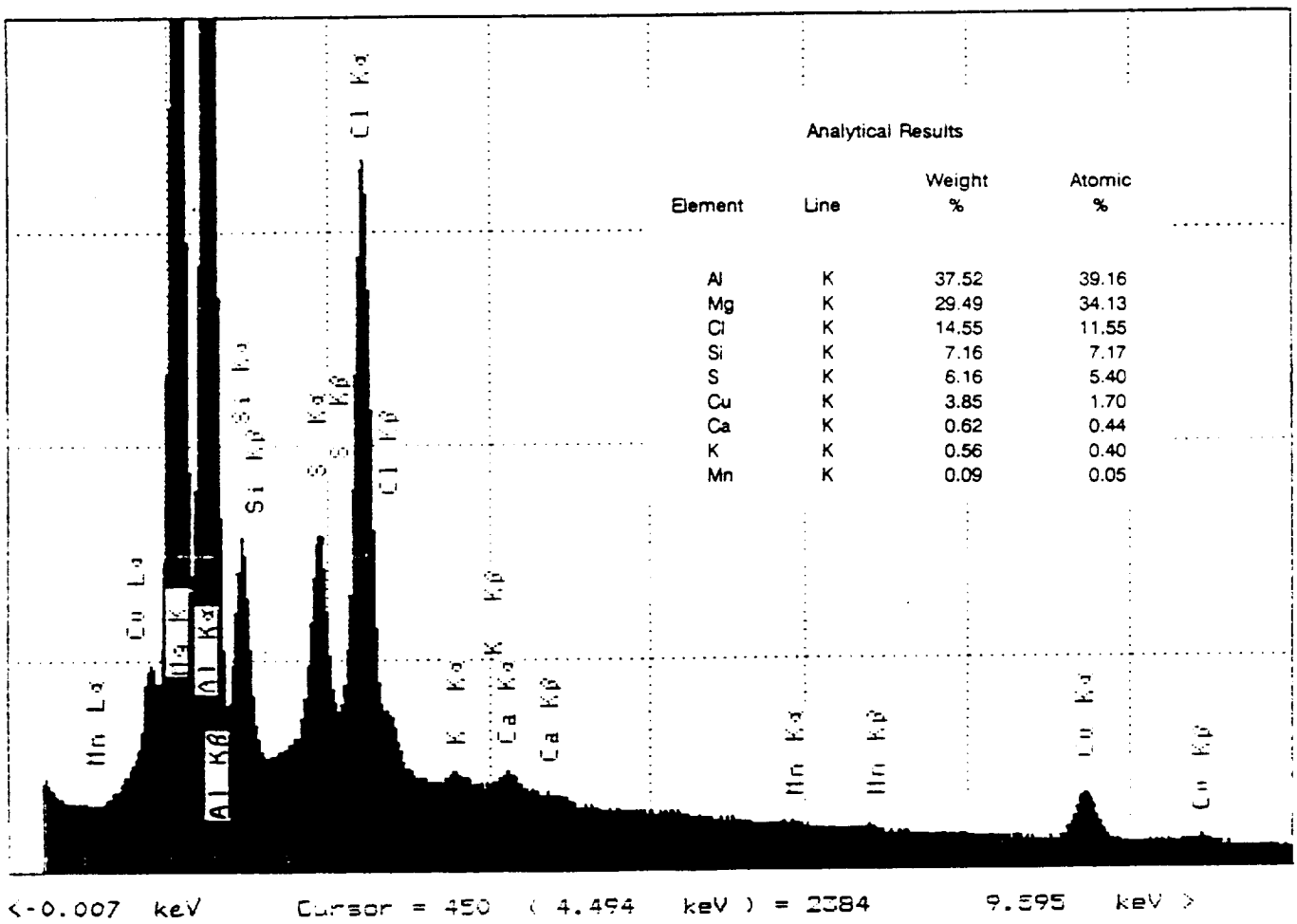

Fig. 22. EDX spectrum atop a large crystal of second phase material (position 1 in Fig. 21(a)). The major elemental constitutents are Al, Mg, and Cl. No Na is observed, in contrast to seawater exposures at T = 30 C and T = 60 C.

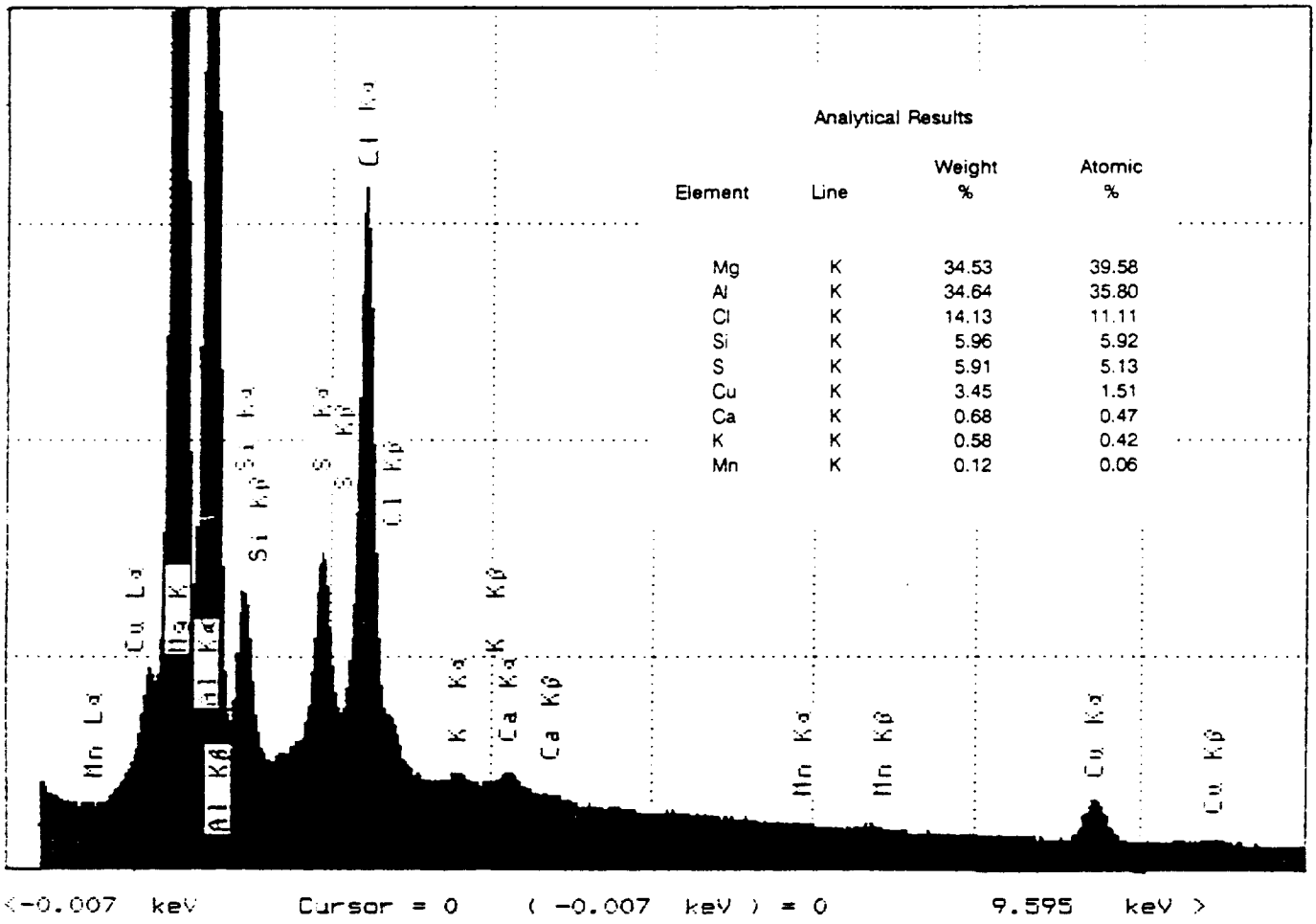

Fig. 23. EDX spectrum atop the corrosion products at position 2 in Fig. 21(a). The major elemental constituents are Mg, Al, and Cl. No Na is observed, in contrast to seawater exposures at T = 30 C and T = 60 C.

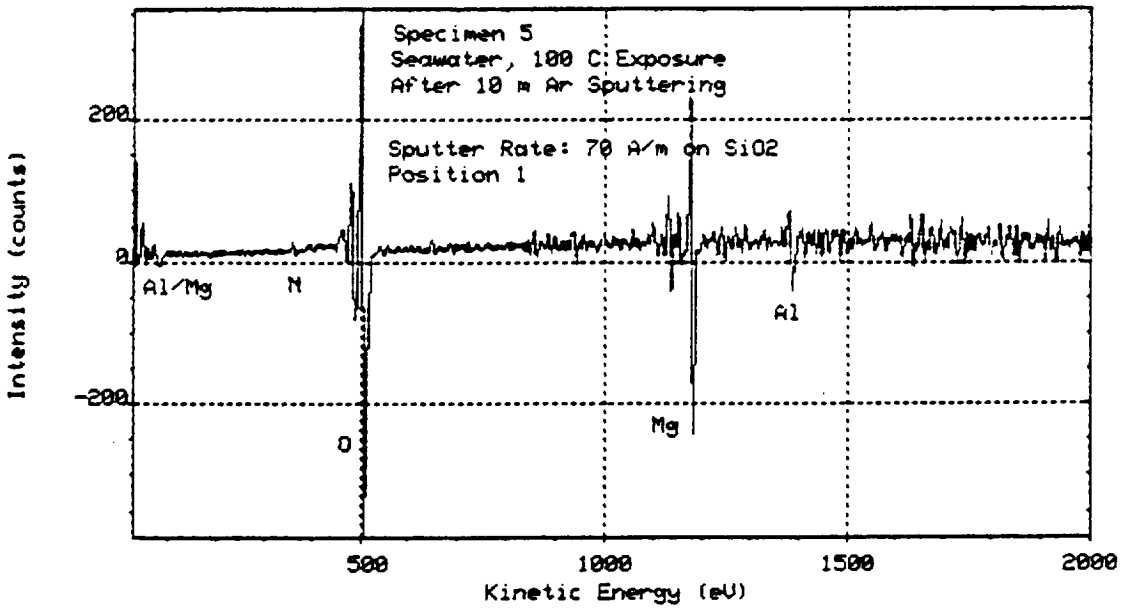

Fig. 24. Auger spectrum atop the T = 100 C reaction surface. Exposure at higher temperature favors formation of MgO. The specimens were Ar sputtered for 10 minutes beforehand to remove traces of adsorbed residual atmospheric gases.

Differences in the corrosion process for 2219 aluminum at different temperatures may be characterized from four viewpoints: pH, weight gain, elemental composition, and crystalline microstructure. We summarize the differences in Table III. All indications point to greater reaction and precipitation of second phase material with temperature, as expected.

Table III

Differences in Seawater Corrosion Characteristics vs Temperature

Property	Temperature		
	T = 30 C	T = 60 C	T = 100 C
Seawater pH Gain	+0.2	+0.2	+0.9
Al Weight Gain (g)	+0.00005	+0.00042	+0.00070
Major Elements	Al, Na, Cl, S	Al, Na, Cl, S	Al, Mg, Cl, S
Crystalline Microstructure	Localized Cubic	Extensive Cubic	Extensive Unknown

VI. The 2219 Al-Cu Alloy Exposed to 3.5% Salt Solution

A. 3.5% Salt Solution Exposure at T = 30 C

In these experiments, a standard Pyrex beaker was filled with a 3.5% salt water solution, and the mixture was heated to 30 C by a hotplate/stirrer. The NaCl was obtained commercially (Fisher) and mixed with 200 ml of 20 megaohm DI water. A specimen of 2219 aluminum was then placed into the salt solution for a period of 2 hours. Visible (grey) discoloration of the aluminum was evident after minutes.

An optical micrograph of the 2219 aluminum alloy before and after 2.0 hours of salt solution exposure at T = 30 C is shown in Figure 25. The corrosion products are extensive, and the presence of pit-like features are visible. Dull grey discoloration of the aluminum could be seen after 30 minutes of exposure, and at the same time, bubbles developed over localized portions of the aluminum surface. Figure 25(b) shows that the corrosion products are primarily localized mounds of deposited second phase material. A closer view is shown in Figure 26. Figure 26(a) is a low magnification SEM photograph of the exposed surface. Figure 26(b) is a high magnification photograph. EDX analysis of one of the round structures (possibly where small a small bubble formed during exposure; in any case, position 1 in Fig. 25(b)) is given in Figure 27. The pit interior is mostly Al with small concentrations of P, Cl, and Ar. Outside this feature (position 2 in Fig. 26(b)), the composition is substantially the same, only with a bit more Cl, shown in Figure 28. Again, because the depth of the corrosion products are unknown, it is difficult with EDX to determine how much of the signal originates from corrosion products and how much originates from the underlying 2219 substrate. Since the EDX composition is so close to the EDX spectrum for the 2219 Al by itself, it is likely that most of the X-rays originate from the substrate.

(a)

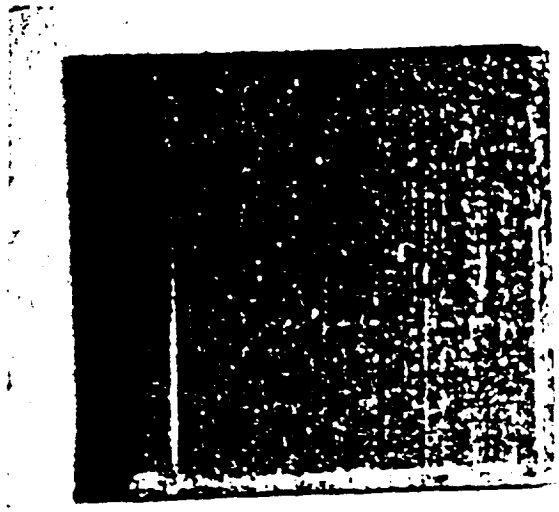

(b)

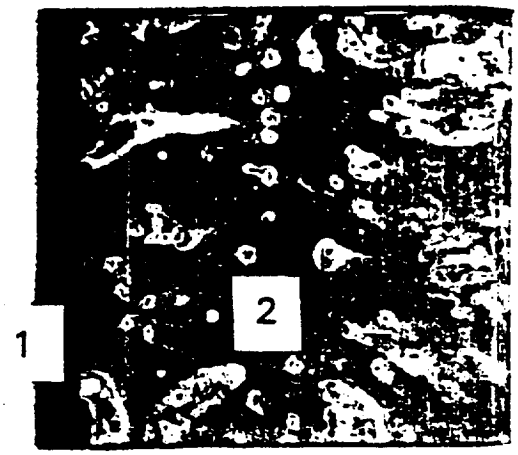

Fig. 25. Optical micrographs of 2219 aluminum (frontside) after 2.0 hours of 3.5% salt solution exposure at T = 30 C. Substantial localized deposition of second phase material is observed.

(a)

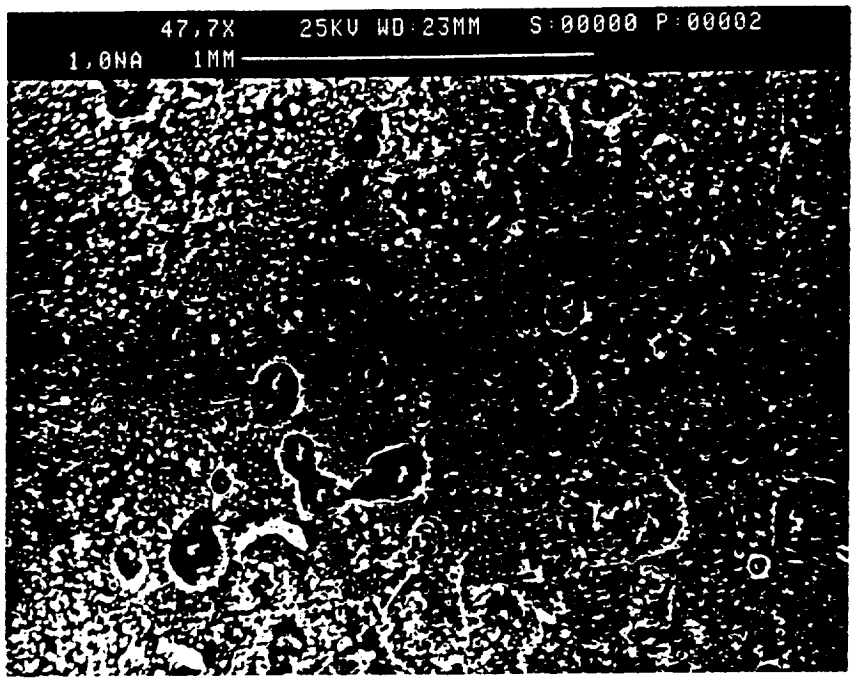

(b)

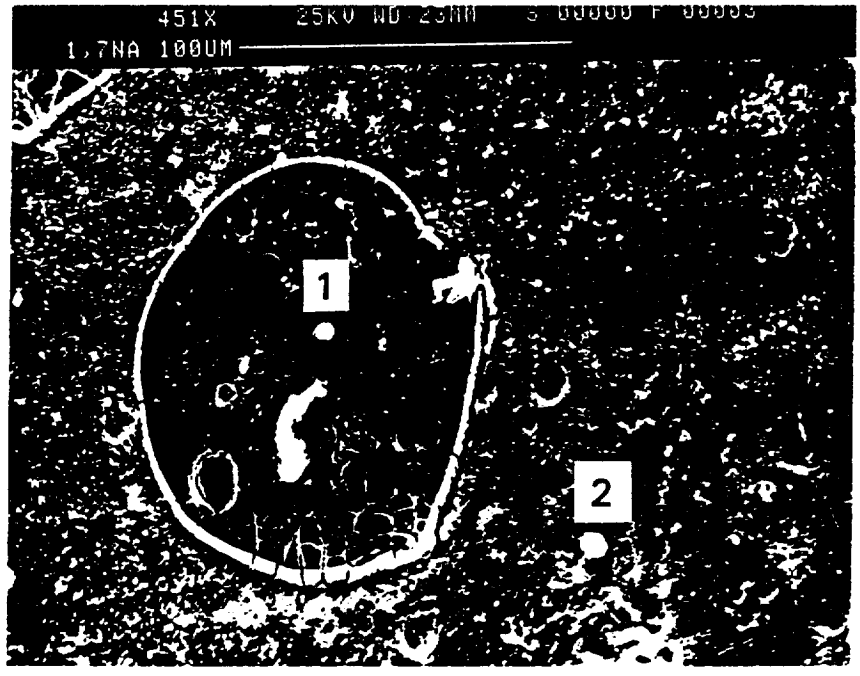

Fig. 26. SEM photographs of the T = 30 C salt solution exposed 2219 aluminum surface. The view in (b) is a blowup of one of the features in (a). Cf. Figs. 7 and 8 to compare corrosion products in seawater at T = 30 C.

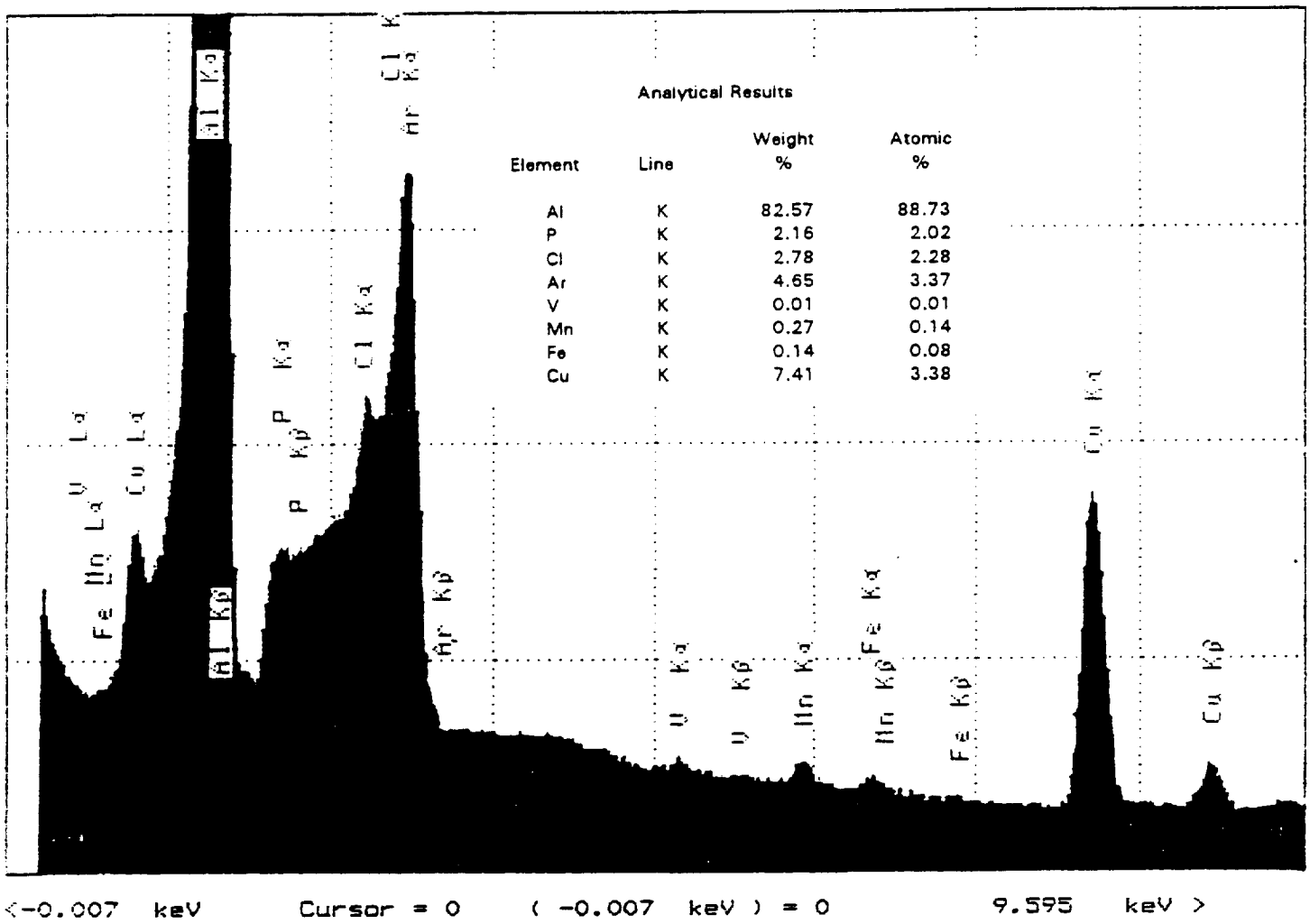

Fig. 27. EDX spectrum inside one of the corrosion features created by 3.5 % salt solution exposure at T = 30 C (position 1 in Fig. 26(b)). The spectrum is similar to the 2219 alloy itself, with the addition of a small amount of Cl (cf. Fig. 3).

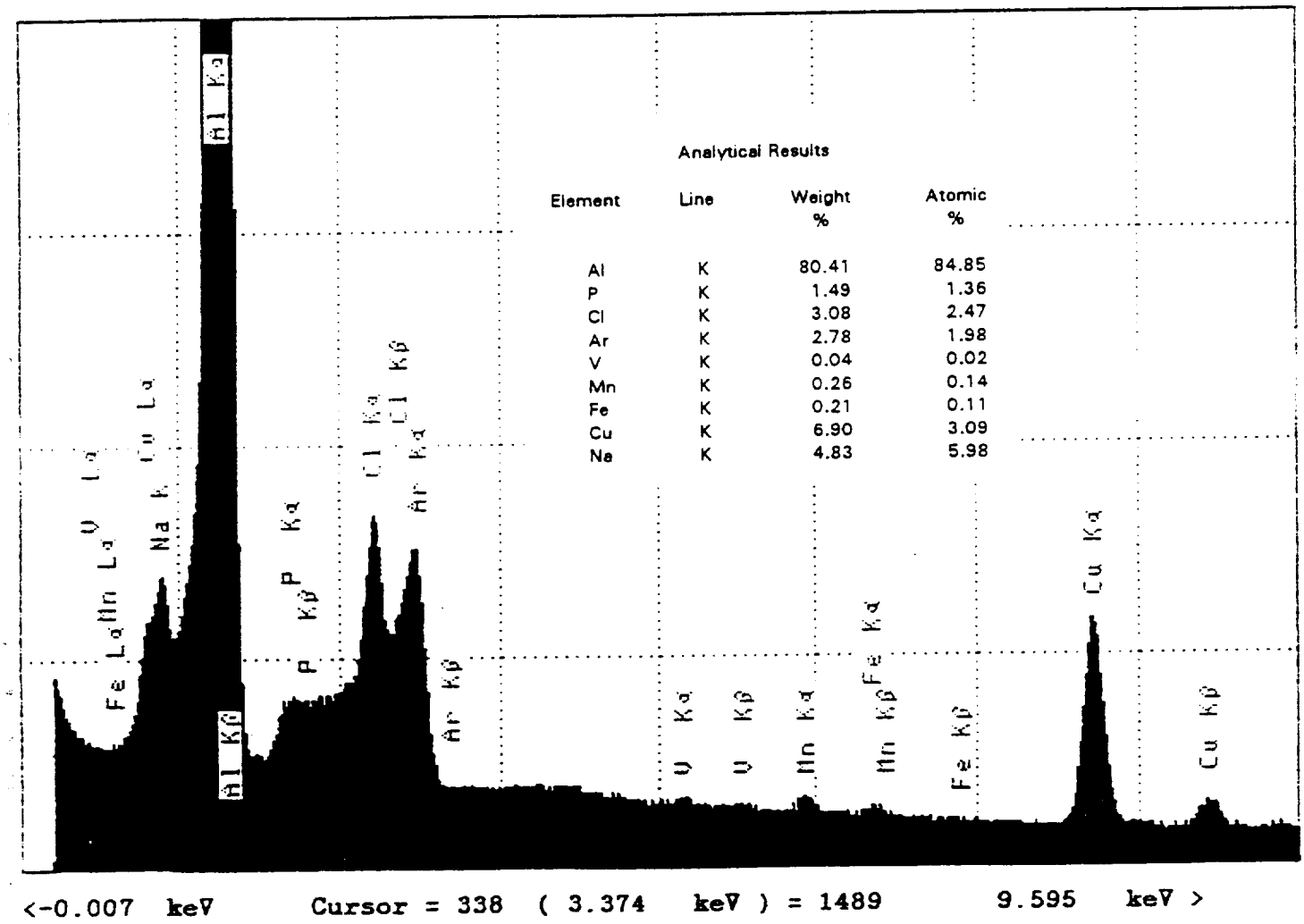

Fig. 28. EDX spectrum alongside one of the corrosion features created by salt solution exposure at T = 30 C (position 2 in Fig. 26(b)). The surface next to the feature contains a larger signal of Cl and the presence of Na.

Auger analysis atop one of the localized mounds (position 1 in Fig. 25) is shown in Figure 29(a). The spectrum demonstrates that the major corrosion product is Al_2O_3, shown by the energies and shapes of the Al Auger peak. Auger analysis off to the side of the mound (position 2 in Fig. 26) is nearly identical to the Auger spectrum on the mound, with the addition of more Na and Cl. The analyses were performed at low incident beam current to minimize the effects of electron stimulated desorption (ESD), discussed above. Accounting for this effect in Auger spectroscopy, and comparing spectra taken by EDX, shows that the predominant reaction mechanism at T = 30 C is growth of Al_2O_3 and NaCl.

The specimen weight and size and the pH of the salt solution was measured before and after the exposure. There was no measureable difference in the size of the 2219 specimen, and no measurable weight change. Since there are obvious deposits of material on the surface, the the material removed by pitting must be counteracted by the deposition weight gain. The pH of the salt solution changed from 7.6 (before) to 8.9 (after) the exposure.

B. 3.5% Salt Solution Exposure at T = 60 C

At T = 60 C, the corrosion is similar to that observed at T = 30 C. There is again evidence of localized pitting, and the surface is covered by second phase material. An optical micrograph of the 2219 aluminum alloy before and after 2.0 hours of exposure at T = 60 C is shown in Figure 30. Dull grey discoloration of the aluminum could be seen after about 15 minutes of exposure, and at the same time, bubbles developed over much of the aluminum surface. Figure 30(b) shows the extent of pitting and a hazy film of material covering the surface.

A high magnification SEM view of the exposed surface is shown in Figure 31. An EDX spectrum over the area-averaged view shown in Fig. 31 is displayed in Figure 32. The composition is roughly the same as for the T = 30 C case, mostly Al, Na, and Cl. Auger analysis atop the hazy film is also shown in Figure 33. The Auger signature is that of Al_2O_3, shown by the energies and shapes of the Al Auger peak. NaCl is also present on the surface because it was observed in EDX, but ESD effects make it difficult to observe. Accounting for this effect in Auger spectroscopy, and comparing

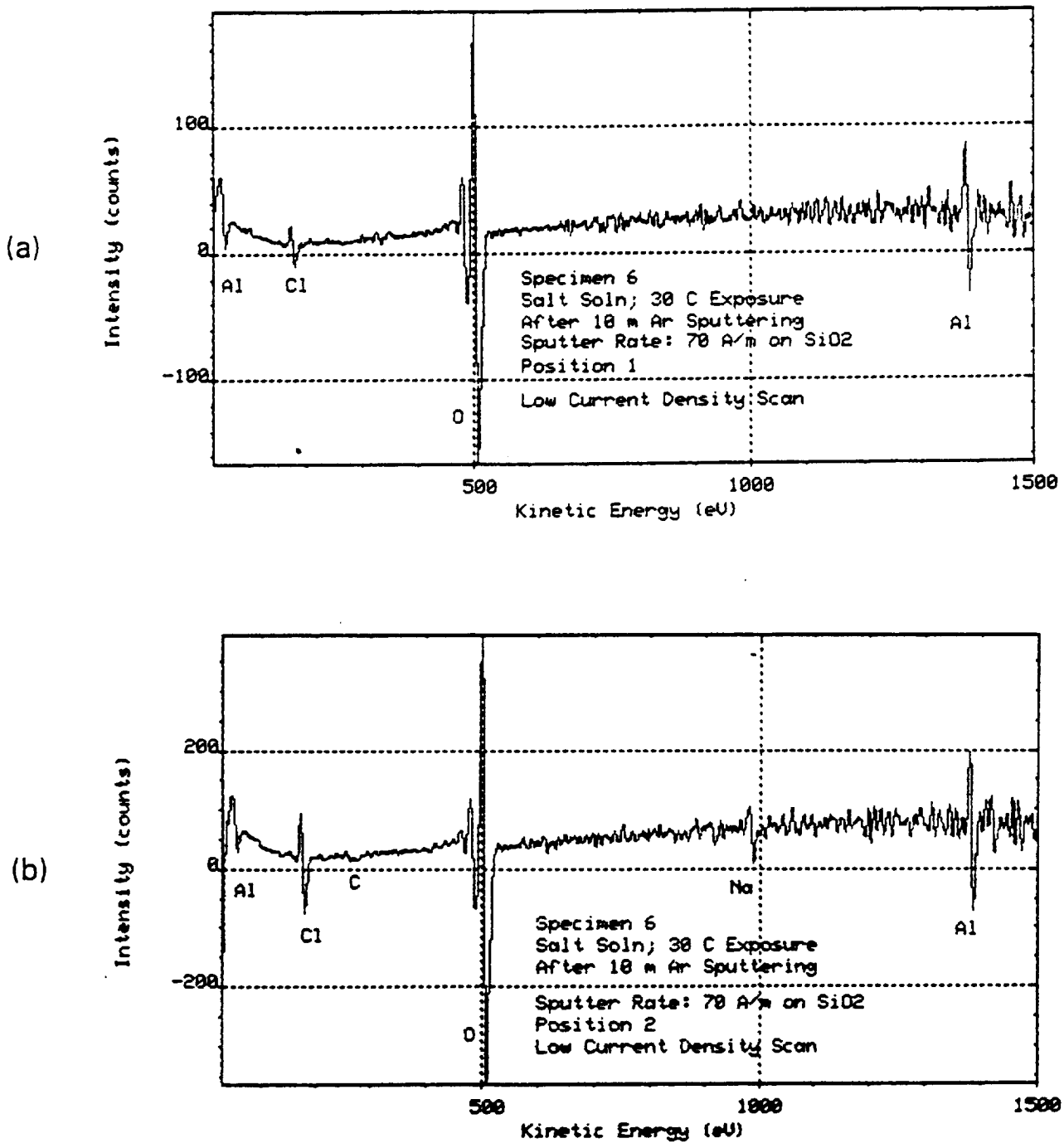

Fig. 29. Auger spectra (a) atop and (b) beside the localized mound in Figure 25 (see positions 1 and 2 in Fig. 25(b)). The Auger signature is that of Al_2O_3, while EDX additionally showed NaCl. The specimen was Ar sputtered for 10 minutes beforehand to remove traces of adsorbed residual atmospheric gases.

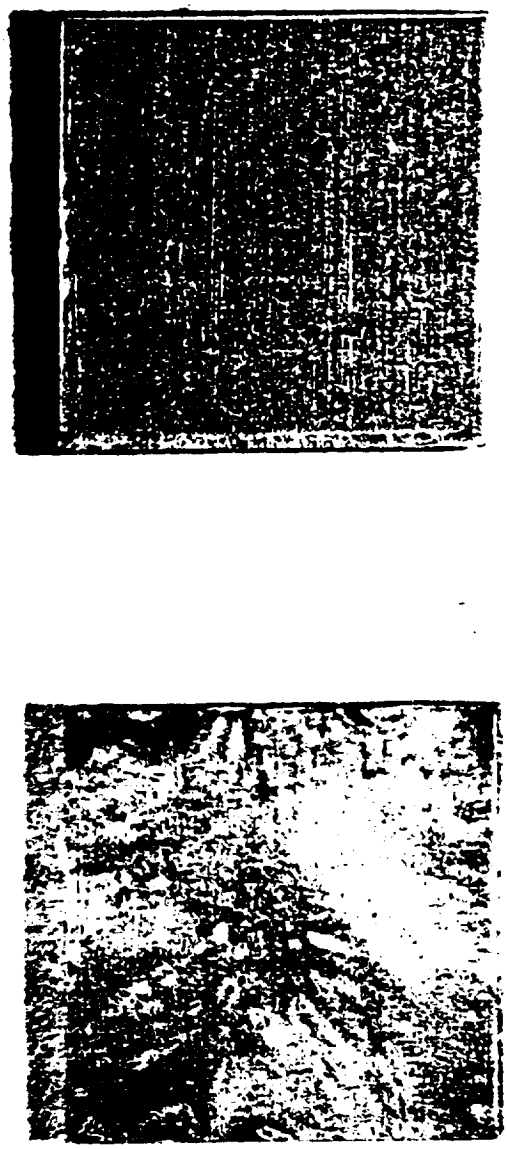

Fig. 30. Optical micrographs of 2219 aluminum (frontside) after 2.0 hours of 3.5% salt solution exposure at T = 60 C. Substantial formation of second phase material is observed.

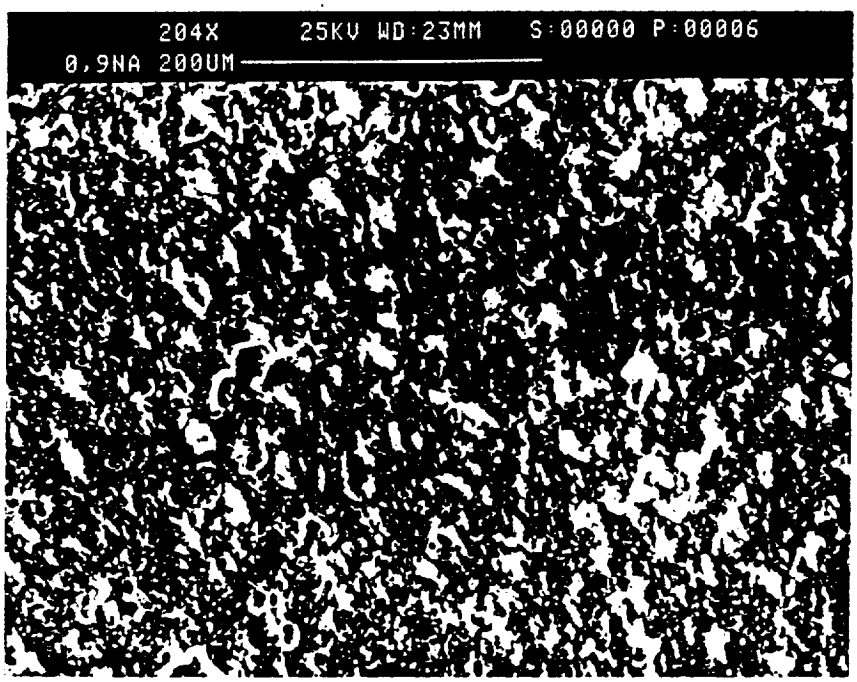

Fig. 31. SEM photograph of the T = 60 C corroded 2219 aluminum, showing the typical appearance of the surface. Cf. Figs. 13 and 14 to compare corrosion products in seawater at T = 60 C. There is less growth of cubic material on the surface exposed to the salt solution.

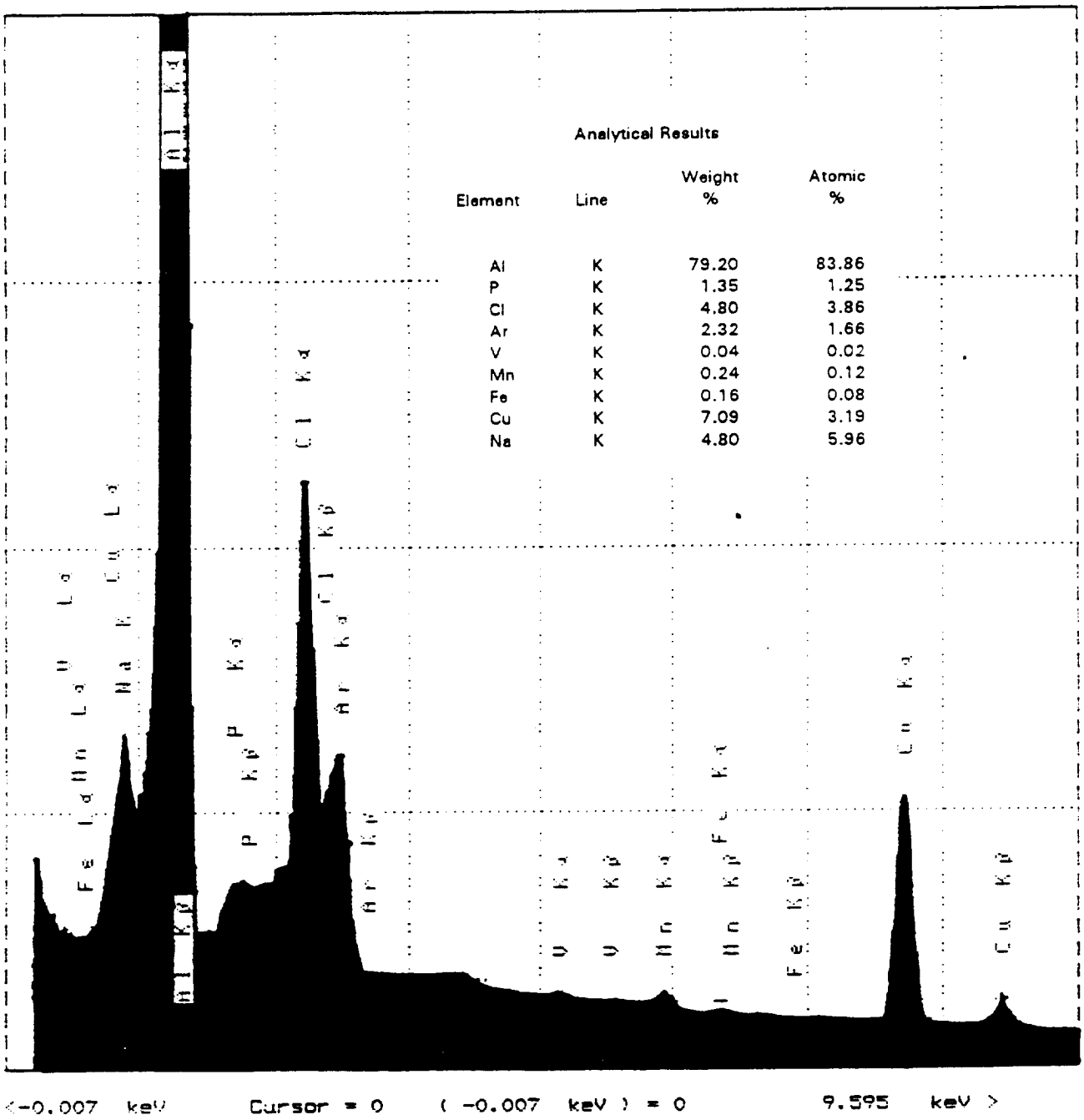

Fig. 32. Area-averaged EDX spectrum over the view shown in Fig. 31. The spectrum is similar to the 2219 alloy itself, with the addition of a small amount of NaCl.

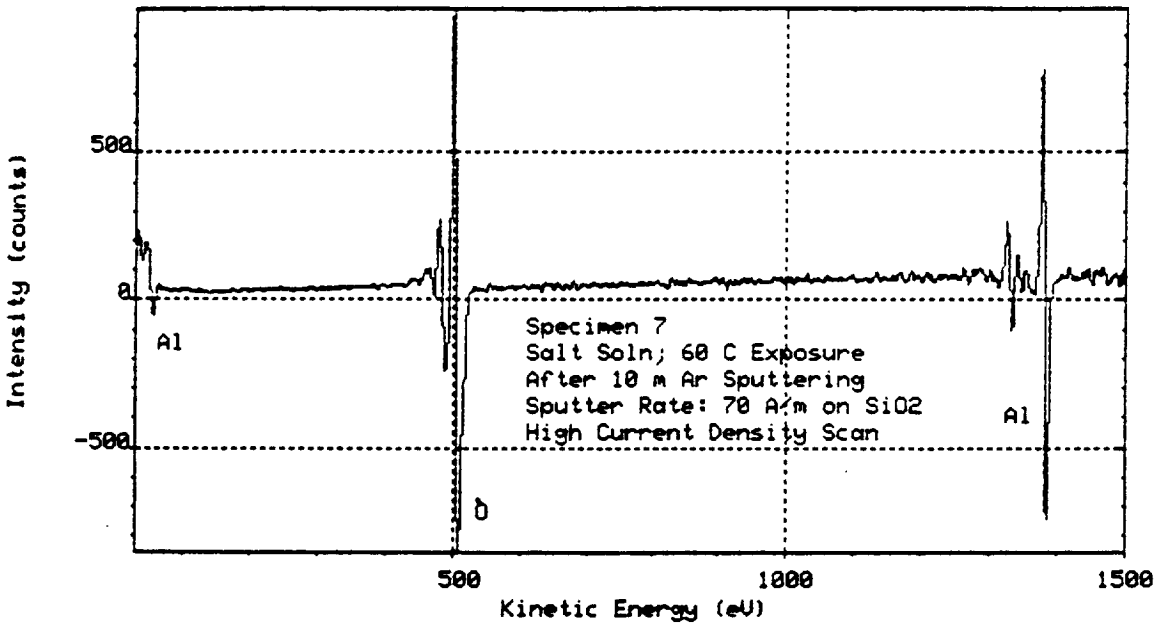

Fig. 33. Area-averaged Auger spectrum over the view shown in Fig. 31. Growth of Al_2O_3 and NaCl dominates, similar to the case at T = 30 C, despite the fact that NaCl is not observed in Auger spectroscopy.

spectra taken by EDX, shows that the predominant reaction mechanism at T = 60 C is growth of Al_2O_3 and NaCl. This is similar to the reaction at T = 30 C.

The specimen weight and size and the pH of the salt solution was measured before and after the exposure. There was no measureable difference in the size of the 2219 specimen, but the weight increased from 0.26221 g before exposure to 0.26245 g after exposure, reflecting the precipitated second phase material. The pH of the seawater also increased, from 7.6 (before) to 8.0 (after).

C. 3.5% Salt Solution Exposure at T = 100 C

In boiling salt solution, 2219 aluminum suffers virtually no corrosion. The surface looks the same before and after the exposure. Only at high magnification are a few salt crystals observed in scattered locations on the surface. Figure 34(a) shows an optical photograph of the surface, which looked the same before and after the exposure. A high-resolution SEM photograph is shown in Fig. 34(b). A few scattered salt crystals are observed.

An EDX spectrum on and beside one of the crystals in Fig. 34(b) is shown in Figures 35 and 36, proving that the crystal are salt. While the crystals are salt, the material beside the crystals is predominantly Al, reflecting the substrate. Auger analysis (not shown) verified that the crystals were NaCl and the substrate was oxidized Al.

The specimen weight and size and the pH of the salt solution seawater was measured before and after the exposure. There was no measureable difference in the size of the 2219 specimen, but the weight increased from 0.25695 g before exposure to 0.26708 g after exposure, reflecting the precipitated NaCl crystals. The pH of the solution also increased, from 7.6 (before) to 8.6 (after).

What is remarkable about this behavior is the lack of reaction. One would expect from chemical kinetics that the corrosion rate would be faster at elevated temperatures. Just the opposite behavior is observed. This shows that simulating corrosion effects in seawater with a 3.5% salt

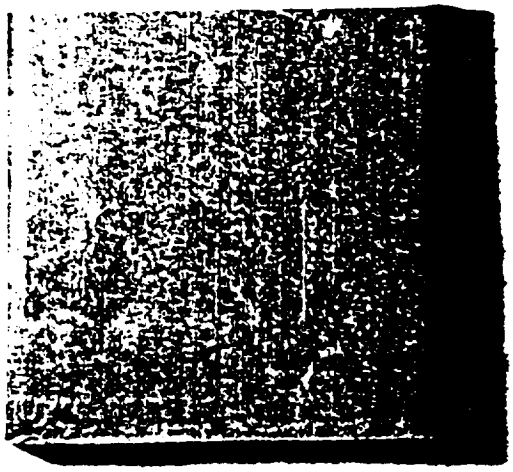

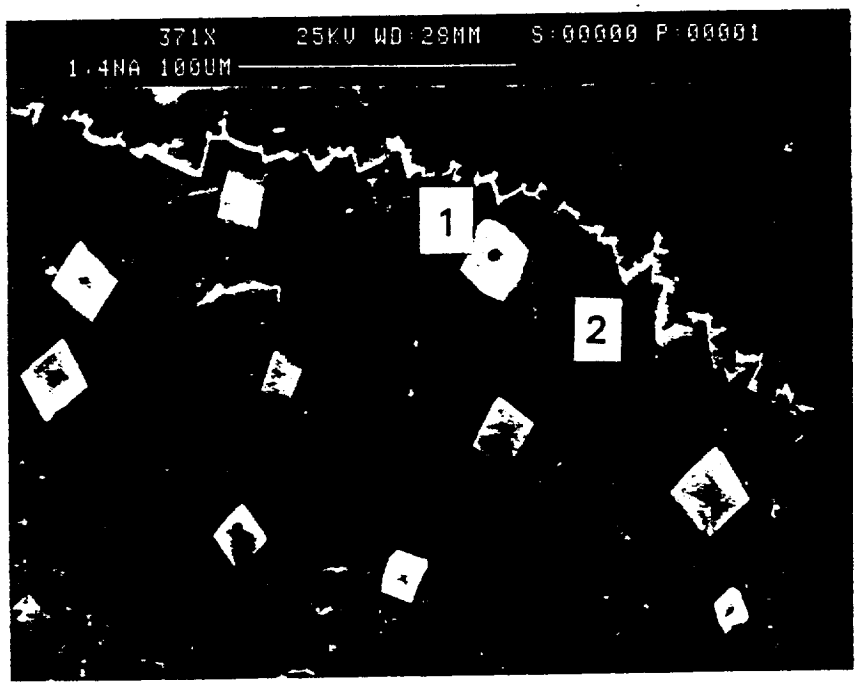

Fig. 34. Optical and SEM micrographs of 2219 aluminum (frontside) after 2.0 hours of 3.5% salt solution exposure at T = 100 C. The optical photograph looks the same before and after the exposure. No corrosion is observed. The SEM photo shows NaCl crystals scattered over the surface.

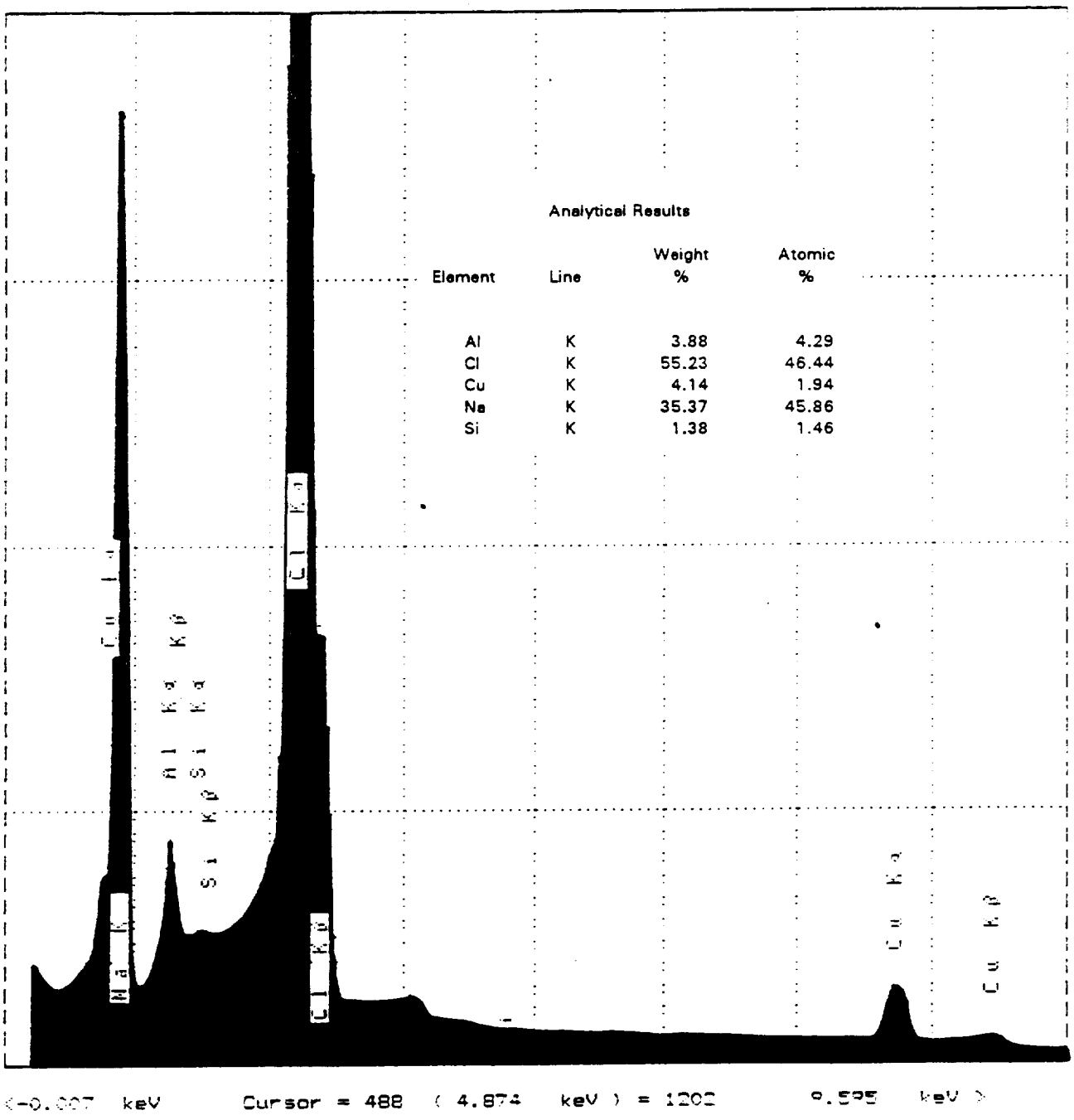

Fig. 35. EDX spectrum atop one of the crystals appearing on the T = 100 C exposed surface (position 1 in Fig. 34(b)). The crystals are NaCl.

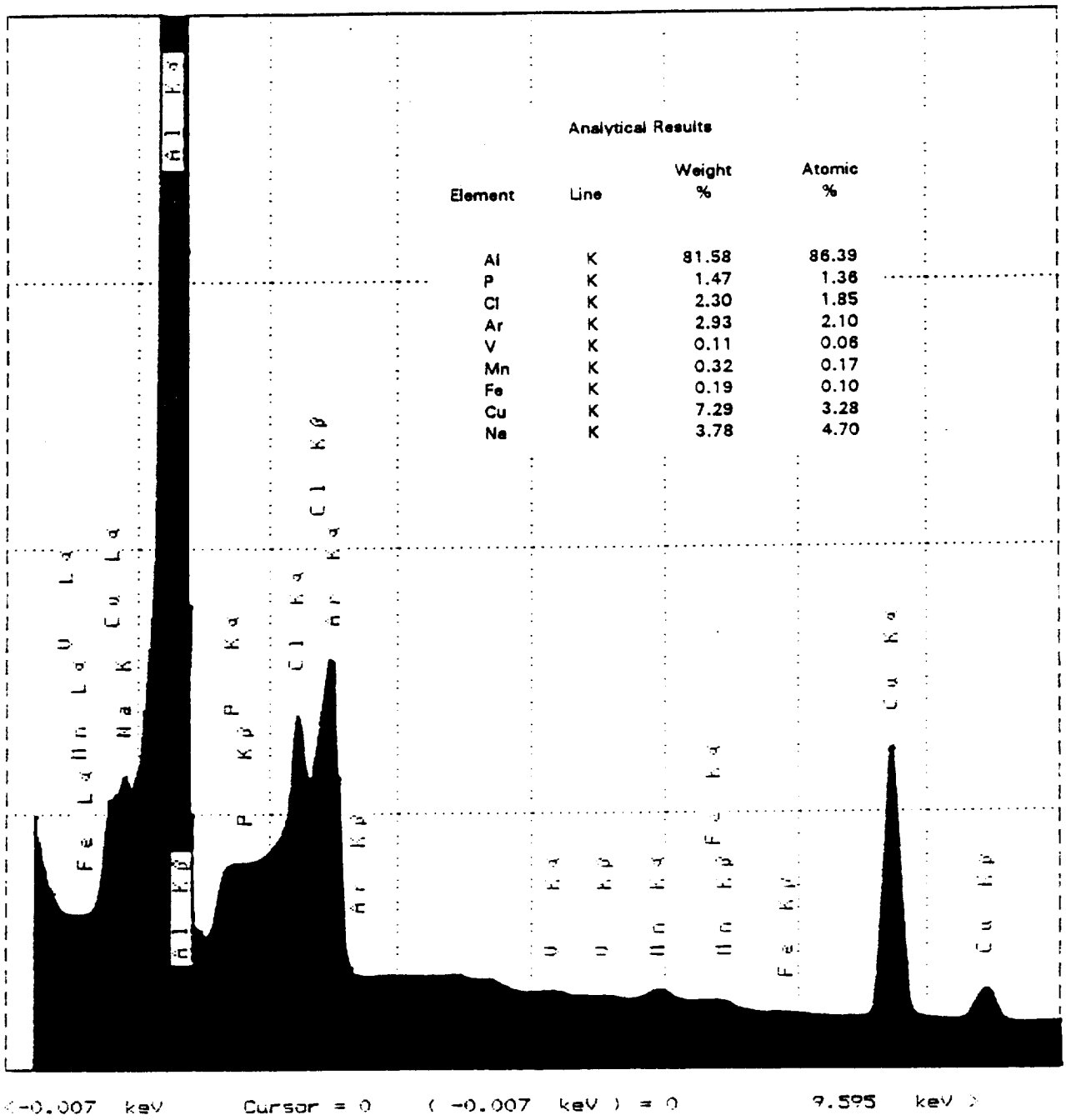

Fig. 36. EDX spectrum alongside one of the crystals seen in Fig 34(b). The spectrum is similar to that for the 2219 alloy itself, with the addition of small amounts of NaCl.

solution is subject to considerable error. Previous tests on 2219 aluminum at T = 100 C showed considerable crystal growth for surfaces in seawater.

D. Salt Solution Exposure Summary

SRB 2219 aluminum was tested for corrosion resistance in a 3.5% salt solution at temperatures of 30 C, 60 C, and 100 C. The corrosion is less extensive at higher temperatures. At 100 C, it is difficult to perceive an observable difference in the metal surface before and after the salt solution exposure. At the lower temperatures, the corrosion consists primarily of pitting and the growth Al_2O_3 and NaCl. Lower temperatures favor formation of Al_2O_3. These results differ from 2219 exposure to seawater where formation of MgO was also observed. The results show that it is not possible to adequately simulate seawater corrosion on 2219 Al with a 3.5% salt solution. This is contrary to what is commonly assumed in the literature.

VII. The 2219 Al-Cu Alloy after Long-Term Seawater Exposure at T = 30 C

An optical micrograph of the 2219 aluminum alloy after 200 hours of seawater exposure at T = 30 C is shown in Figure 37. The temperature of T = 30 C was chosen for the long-term exposure because it is roughly the temperature of Gulf seawater. Extensive growth of second phase material covers the surface. High resolution SEM micrographs of the surface are shown in Figure 38. The streaks seen in photo (b) is due to charging--the deposited material is so thick and insulating.

EDX analysis of regions on and off the second phase mounds is shown in Figures 39 and 40. Since our previous experience with Auger spectroscopy has shown that the growth features are Al_2O_3, MgO, and NaCl, we have assumed these stoichiometries when calculating quantitative EDX compositions in order to determine the amount of each compound present (despite the fact that the EDX technique with our present X-ray window cannot O). In doing so, we assume that the EDX signal is originating entirely from the second phase mounds (a safe assumption here, since the mounds are very thick). The EDX results do not suffer from the effects of electron stimulated desorption (as seen previously in Auger analysis) because most of the EDX signal originates from under the surface).

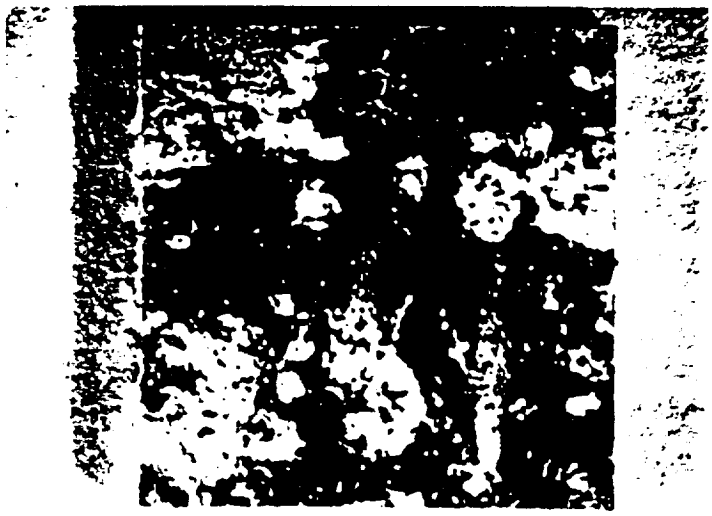

Fig. 37. Optical micrograph of 2219 aluminum after exposure to seawater for 200 hours at T = 30 C.

(a)

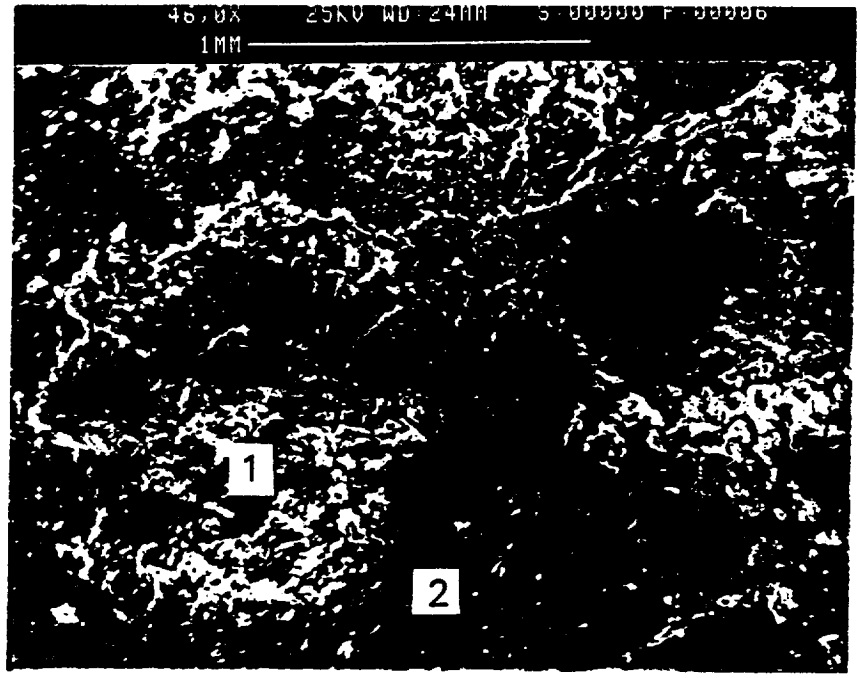

(b)

Fig. 38. Two SEM views atop the 2219 aluminum after exposure to seawater for 200 hours at T = 30 C. Micrograph (a) was taken at the right side of Fig. 37, while micrograph (b) was taken at the left side of Fig. 37.

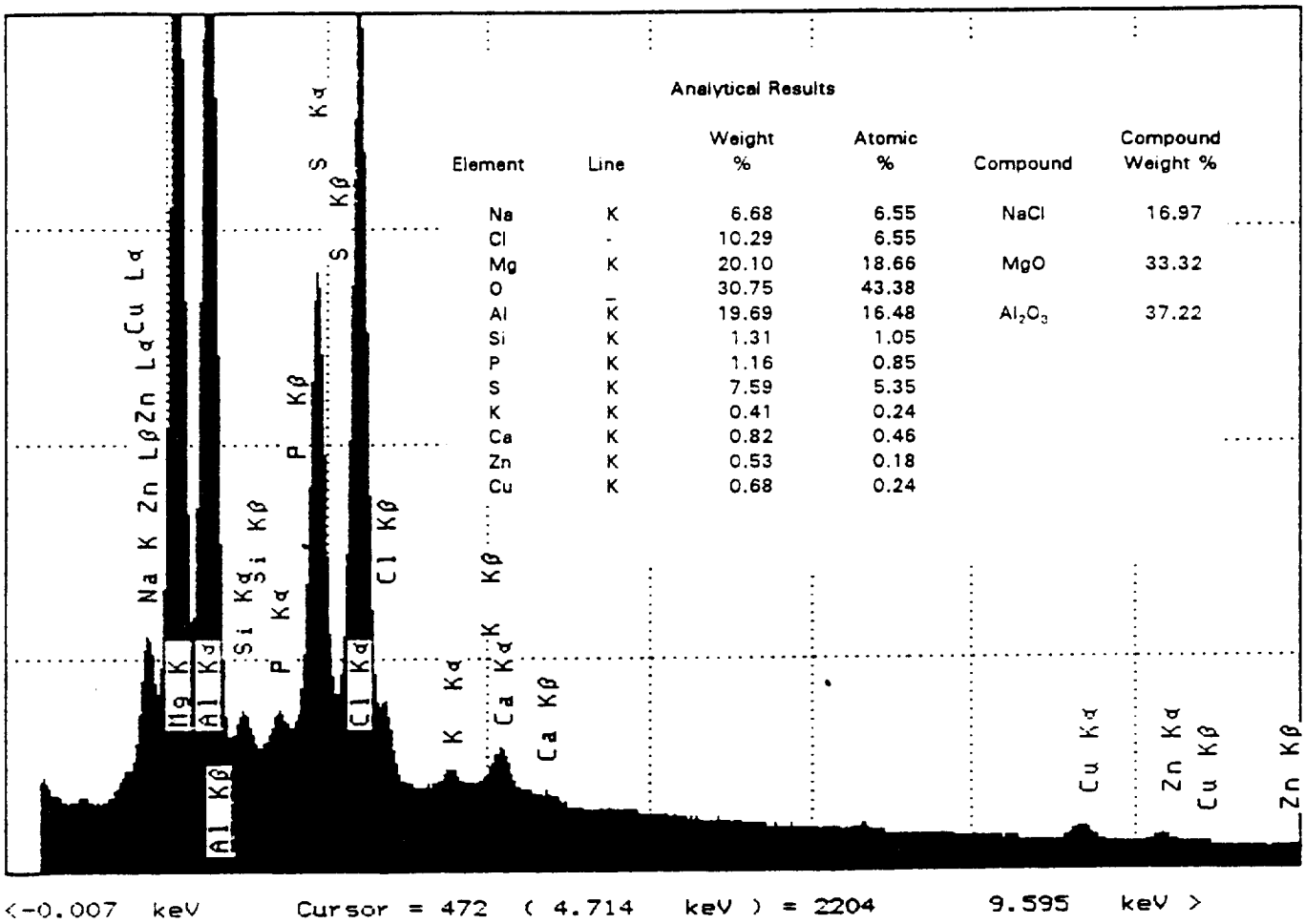

Fig. 39. EDX spectrum atop the localized mound in Figure 38(a). See position 1 in Fig. 38(a). The second phase material is mostly Al_2O_3, MgO, and NaCl.

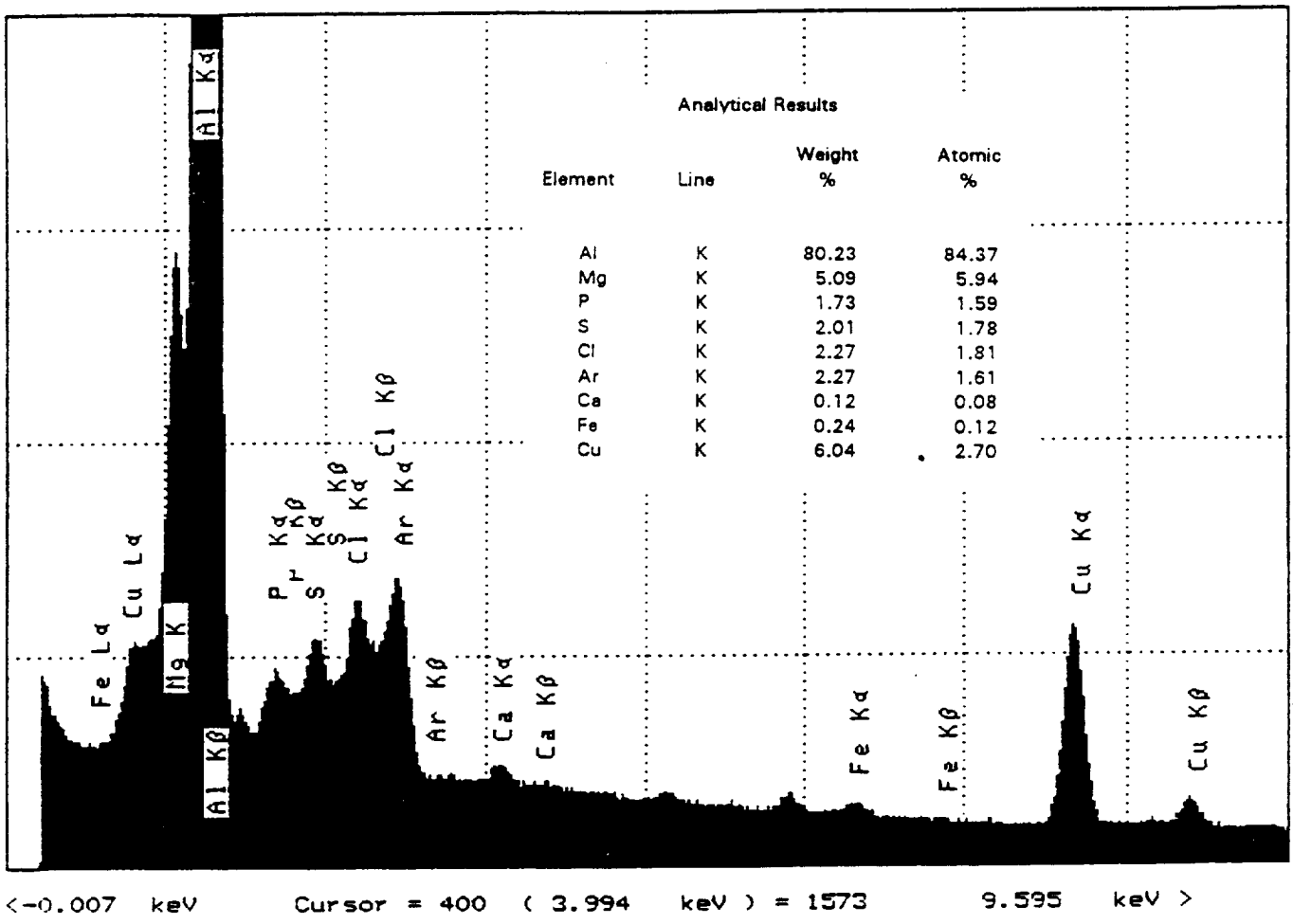

Fig. 40. EDX spectrum off to the side of the localized mound in Figure 38(a). See position 2 in Fig. 38(a). A thin film of precipitated Al_2O_3, MgO, and NaCl is indicated, but the incident beam penetrates through it so most of the detected signal is from the underlying 2219 Al substrate.

The EDX composition of the second phase mounds (position 1 in Fig. 39) shows that the large mounds are composed of (by weight %): 1/3 Al_2O_3, 1/3 MgO, 1/6 NaCl, and 1/6 other elements. EDX analysis off to the side of one of the mounds (position 2 in Fig. 3) shows small amounts of Na, Mg, and Cl, indicating that growth of Al_2O_3, MgO, and NaCl has occured in a thin film that the incident electron beam has penetrated. Since the film is so thin in this location, most of the EDX signal at this position originates from the 2219 substrate and is mostly Al. That a thin film of Al_2O_3, MgO, and NaCl exists on seawater-exposed specimens was shown in previous Auger work.

The specimen weight and size and the pH of the seawater was carefully measured before and after the exposure. There was no measurable difference in the size of the 2219 specimen, but the weight increased from 0.26701 g before exposure to 0.26823 g after exposure, reflecting the precipitated second phase material on the aluminum. The weight gain of +0.00122 g is higher than the weight gain of +0.00005 g during 2 hours of seawater exposure, showing that more second phase material is precipitating with exposure time. The pH of the seawater also increased by +0.22 which was roughly the same as the pH change after 2 hours of seawater exposure, reflecting a decrease in $[H^+]$.

In summary, long-term (200 hours) exposure of 2219 Al to seawater at T = 30 C showed little fundamental differences from the case of short-term (2 hours) exposure of 2219 Al to seawater at the same temperature. In both instances, substantial formation of Al_2O_3, NaCl, and MgO is observed atop the alloy surface. There is more precipitated material at the longer exposure, but no new growth features are observed.

VIII. Conclusions

It is not unexpected that the major corrosion products observed when aluminum is exposed to seawater are Al_2O_3 and NaCl. The presence of MgO on seawater-exposed aluminum at high temperature is less expected but not surprising. Each of these compounds have low Gibbs free energies of formation and will form readily if the correct kinetic conditions exist.

The question arises whether this is all bad. The answer depends on how one defines bad. As discussed above, the presence of an oxide layer on aluminum is one of the primary ways it is protected against corrosion. In this sense, the oxide layer is good because, once formed, it protects against further corrosion. From other viewpoints however, (e.g., an asthetic viewpoint), the formation of lumps of Al_2O_3 on formerly shiny aluminum may be undesirable.

The presence of pitting and lifting is more serious. If allowed to proceed unchecked, these pitting and lifting will degrade the strength of the alloy and lead to service failure and/or short life. In order to reduce such effects, the following suggestions are offered.

There are seven basic approaches to the prevention of metallic corrosion, listed in the approximate order of utility for protecting aluminum: 1) Choice of a more resistant alloy; 2) Improvement in equipment design; 3) Cathodic protection by use of cladding and sacrificial anodes; 4) Choice of metal coating; 5) Choice of inhibitors; 6) Alteration of environment; and 7) Use of nonmetallic coatings (e.g., rubber). We will discuss each of these from the point of view of SRB corrosion.

A. Choice of Alloy

Workers who are experienced with aluminum alloy corrosion admit that the most common problem in Al-Cu corrosion is the use of Al-Cu alloys in corrosive environments without adequate protective measures. For example, in cases where Al-Cu alloys would be expected to perform satisfactory, it was found that the alloys had been damaged in some way in the service environment. There are numerous examples of underframes in buses and trucks, made of the Al-Cu alloy, which are softened for bending by heat treatment with a blowtorch. Such pieces are corroded only in the heated zone. It is possible that this corrosion mechanism may be occurring in 2219

SRB applications due to the high temperatures within the booster. Steel rivets driven hot through Al-Cu structural members cause blistering of the aluminum alloy in corrosive atmospheres. Heating also causes precipitation of $CuAl_2$ in the grain boundaries, with resultant development of intergranular corrosion. A materials analysis of the Al-Cu alloy from a spent booster would be helpful to clarify the corrosion mechanism.

A better choice of alloy may be the Al-Mg alloys which appear to offer the best combination of strength and corrosion resistance, and are preferred for structural purposes in corrosive environments. These alloys are widely used, for example, in the construction of boats and ship superstructures, especially AA-5052 and AA-5083 alloys. Cast alloys J and K both have good resistance to corrosion, but alloy K, especially after aging in service, begins to develop stress corrosion and should not be employed in a stressed condition in a corrosive environment.

B. Improvement in Equipment Design

The most common design failures encountered with aluminum structures in service involve galvanic corrosion between rivets and the aluminum and crevice corrosion, both of which are well understood and can be avoided. Some general rules that apply are: 1) Select combinations of metals as close together as possible in the galvanic series; 2) Use cathodic fastenings and avoid combinations with an unfavorable ratio of anode to cathode area; 3) Provide good electrical insulation of the two metals, by using gaskets, fibers, sleeves; 4) If paint can be applied, always paint at least the cathode. If only the anode were painted a break would give an unfavorable ratio of anode to cathode area and lead to rapid attack at the break; 5) Install small replaceable heavy sections of the anodic metal at joints if possible; 6) Make the dissimilar metal contact out of the corrosive environment if possible; and, 7) Increase the thickness of the anodic metal. The scope of this project did not include the investigation of galvanic corrosion.

C. Cathodic Protection

The NACE has published a paper which tentatively recommends certain methods for the cathodic protection of aluminum in waters and soils [24]. It is difficult to see how this could be applied to an SRB, but the reader may

wish to consult this paper if interested.

D. Application of Coatings

Paint is usually applied to aluminum for esthetic reasons rather than for the prevention of corrosion; however, it is difficult to imagine a paint which would be able to withstand the hostilities of a SRB. Popular baked enamels include vinyls and acrylics. A more feasible coating method would be to take advantage of the ability of aluminum to oxidize. The thin oxide film present on the surface of aluminum can be thickened roughly 500 times (to ~ 0.04-0.08 mils) by immersion in various hot acid and alkaline solutions. The films produced are mainly Al_2O_3, but frequently contain chemicals to render them more corrosion resistant. Several proprietary chemical coatings exist; the trade names are: Alodine (Amchem), Bonderite (Hooker), and Iridite (Allied Research). Much thicker (0.3-1.0 mil) oxide films can be produced by electrochemical treatment in certain solutions. Anodic films to prevent corrosion of aluminum are commonly found on automobile trim and building facades. The most common electrolyte used to anodize aluminum is H_2SO_4 (15% concentration). Applying metallized coatings to aluminum has not been widely used, primarily due to cost.

E. Use of Aluminum Inhibitors

The use of inhibitors to prevent the corrosion of aluminum has been reviewed by Mears and Eldredge [25], Haygood and Minford [26], and Roebuck and Pritchett [27]. Since inhibitors are typically used in recirculating and/or small volume systems, and the ocean environment is so vast, inhibitors will not be considered further here.

F. Alteration of the Environment

It is sometimes possible to alter the agressiveness of an environment by altering it in one way or another. Since this is not possible in an ocean environment, it will not be discussed further.

G. The Effects of Rinsing

Since most of the corrosion products are Al_2O_3, NaCl, and MgO, we wanted to see if the effect of rinsing the aluminum specimens with a high pressure stream of DI water, similar to the way in which people who live in northern climates rinse salt off their cars in winter to retard corrosion. It does appear to be possible to rinse some of the corrosion products off the 2219 Al with a jet of water. This was observed when we subjected the corroded 2219 Al specimen to a jet spray of DI water from a standard laboratory spray nozzle for 5 minutes. It was found that some of the crystalline material had vanished after the rinse (e.g., the crystalline stringer seen in Fig. 19), but the bulk of the material remained. The was confirmed in the weight loss of the 2219 sample before and after the rinse. Before the rinse, the specimen weighed 0.26346 g. After the rinse, the specimen weighed 0.26333 g, reflecting a 0.00013 g loss during rinsing. Hence, rinsing an SRB immediately after recovery may help to retard the corrosion process.

IX. References

[1] W. E. Tragert, U.S. Atomic Energy Commission Report TID 7587, 121 (1960).

[2] V. H. Troutner, U.S. Atomic Energy Commission Report HW 51849, September 30, 1957.

[3] M. S. Hunter and P. Fowle, J. Electrochem. Soc. 103, 482 (1956).

[4] R. K. Hart, Trans. Faraday Soc. 53, 1020 (1957).

[5] L. J. Barker and H. P. Godard, unpublished work, 1960.

[6] P. Mabb, Metallurgia 13, 109 (1936).

[7] R. L. Moore, Eng. News Record 135(16), 124 (1945).

[8] R. B. Spacht, J. Chem. Educ. 23, 253 (1946).

[9] P. F. Thompson, J. Council Sci. End. Res. (Australia) 15, (1946).

[10] O. L. Mitchell, Mat. Meth. 23, 457 (1946).

[11] E. H. Dix, Corrosion of Metals, American Society for Metals (1946).

[12] R. B. Mears, Corrosion Handbook, ed. H. H. Uhlig, Wiley, New York (1946).

[13] Anon., Sheet Met. Ind. 24, 1633 (1947).

[14] S. Wernick, Sheet Met. Ind. 26, 806 (1949).

[15] H. P. Godard, Corrosion 11, 542 (1955).

[16] E. H. Dix Jr., R. H. Brown, and W. W. Binger, Metals Handbook, 8th ed., p. 916 (1961), American Society for Metals.

[17] H. Kaeschke, Werk. und korr 14, 557 (1963).

[18] Anon., Aluminum World 1, 1 (1894).

[19] Anon., Aluminum World 1, 201 (1895); 2, 49 (1895); 2, 157, 217 (1896); 5, 26 (1898); 7, 29 (1900); 7, 93 (1901); J. Soc. Chem. Ind. 1895, p. 487; Proc. Inst. Mech. Engrs. 55, 347 (1898).

[20] H. P. Godard and F. F. Booth, Congres International de la Corrosion Marine et des Salissures, Editions du Centre de Recherches et l'Etudes Oceaniques, 1 Quai Branly, Paris 7 (1965).

[21] T. E. Wright and H. P. Godard, Corrosion 10, 195 (1954).

[22] H. P. Godard, unpublished work (1959).

[23] L. E. Davis, P. W. Palmberg, et. al, Handbook of Auger Electron Spectroscopy, (Eden Prairie: Physical Electronics Division, Perkin-Elmer Corp.), 1976.

[24] N.A.C.E. Technical Unit Committee T-2M, Mater. Prot., 2(10), 106 (1963).

[25] R. B. Mears and G. G. Eldredge, Ind. Eng. Chem. 27, 736 (1945).

[26] A. J. Haygood and J. D. Minford, Corrosion 15, 20 (1959).

[27] A. H. Roebuck and T. P. Pritchett, Mater. Prot. 7(5), 16 (1966).